DOUBLE NEGATIVE NANO-STRUCTURED METAMATERIAL ABSORBER FOR SOLAR THERMO-PHOTOVOLTAIC SYSTEMS

by

MINHAZUL KARIM

MD. MEHRABUL AMIN MOLLA

BACHELOR OF SCIENCE IN ELECTRICAL AND ELECTRONIC ENGINEERING

Department of Electrical and Electronic Engineering
INTERNATIONAL ISLAMIC UNIVERSITY CHITTAGONG

MAY 2021

DOUBLE NEGATIVE NANO-STRUCTRURED METAMATERIAL ABSORBER FOR SOLAR THERMO-PHOTOVOLTAIC SYSTEMS

by

MINHAZUL KARIM

MD. MEHRABUL AMIN MOLLA

A thesis/project
submitted as partial fulfilment of the requirement for the degree of

BACHELOR OF SCIENCE IN ELECTRICAL AND ELECTRONIC ENGINEERING

Department of Electrical and Electronic Engineering
INTERNATIONAL ISLAMIC UNIVERSITY CHITTAGONG

MAY 2021

CERTIFICATE OF APPROVAL

The thesis/project entitled as "**Double Negative Nano-structured Metamaterial Absorber For Solar Thermo-Photovoltaic Systems**" submitted by **Minhazul Karim**, bearing Matric ID. **ET163075** and **Md. Mehrabul Amin Molla**, bearing Matric ID. **ET163082** of session **Spring 2020**, to the Department of Electrical and Electronic Engineering, International Islamic University Chittagong, has been accepted as satisfactory in partial fulfilment of the requirements for the degree of Bachelor of Science in Engineering and approved for the examination held on **28th May, 2021**.

_____

Supervisor
Dr. Sikder Sunbeam Islam
Associate Professor,
Department of Electrical and Electronic Engineering,
International Islamic University Chittagong.

DECLARATION

It is hereby declared that this work has been done by us and no portion of the work contained in this thesis/project has been submitted elsewhere for the award of any degree or diploma.

_____

Minhazul Karim

_____

Md. Mehrabul Amin Molla

ACKNOWLEDGMENT

All praises and thanks to Allah, the Lord of the world, the most Beneficent, the most Merciful for helping us to accomplish this work.

Firstly, we would like to express our cordial thanks and gratitude to our supervisor Dr. Sikder Sunbeam Islam who gave us the golden opportunity to do this wonderful research work. This thesis helped us in doing a lot of research and we came to know about so many new things. We are really thankful to him.

Secondly, we would also like to thank our parents and seniors who helped us a lot in finalizing this thesis within the limited time frame.

Authors

ABSTRACT

A double negative nano-structured polarization insensitive perfect metamaterial absorber (PMA) is observed and substantiated for solar photo-voltaic systems. This kind of absorbers with high fractional bandwidth (FBW) are currently drawing massive interest throughout the research of optics. Specially in solar harvesting metamaterial absorbers can give a huge boost in efficiency by intensifying the solar electromagnetic wave. Visible wavelength has been the key focus of the proposed design so that the structure can utilize solar energy proficiently. Aluminium and Gallium Arsenide have been chosen as material for their higher electron mobility along with temperature stability. Enormous parametric inspections have been carried out for proper characterization of the PMA absorber and relating the physics laying behind the results have been explained. Finite Integration Technique (FIT) is used in simulation to perform the characterization and calculation of absorbance and reflectance from scattering parameters. The metamaterial shows almost 99.86%, 98.87%, 97.61% and 99.84% perfect absorption at 677.6 THz, 624.8 THz, 560 THz and 522.4 THz resonance frequencies at 0° polarization angle. In all three modes of waveguide propagation such as Transverse Electromagnetic (TEM), Transverse Electric (TE) and Transverse Magnetic (TM) mode the designed model shows similar absorbance. The insensitivity of polarization angle has also been verified. So, the proposed metamaterial absorber exhibits proper absorption for optical ranges and can be used for solar photo-voltaic systems.

TABLE OF CONTENTS

LIST OF FIGURES

LIST OF TABLES

LIST OF ABBREVIATIONS

CST MWS	Computer Simulation Technology Microwave Studio
CST	Computer Simulation Technology
EM	Electromagnetic
FBW	Fractional Bandwidth
FIT	Finite Integration Technique
FSS	Frequency Selective Surface
HAADF	High Angle Annular Dark Field
MMA	Metamaterial Absorber
PEC	Perfect Electric Conductor
PEMC	Perfect Electromagnetic Conductor
PMA	Perfect Metamaterial Absorber
PMC	Perfect Magnetic Conductor
PML	Perfectly Matched Layer
STEM	Scanning Transmission Electron Microscopy
STPV	Solar Thermophotovoltaics
TE	Transverse Electric
TEM	Transverse Electromagnetic
TM	Transverse Magnetic

CHAPTER 1
INTRODUCTION

1.1 Introduction

Solar energy is a suitable destination amongst other sustainable power resources to produce more power with the help of photovoltaic cells. Power carried by the solar radiations within one hour can produce yearly power utilization of the World [1]. However, the problem is that there is no satisfactory method to utilize this resource. Metamaterial innovation can be implemented to undertake the subject of Solar energy harvesting can be taken charge of by the implementation of viable construction of more efficient absorbers. Negative permeability, left-handed properties, negative refraction and evanescent wave amplification which cannot be found in natural materials [2], [3], invisible cloaks [4], perfect lens [5], and a perfect absorption [6] are the remarkable properties of metamaterial, which are absolutely necessary for the employment of perfect metamaterial absorbers [7].

1.1.1 Energy Crisis

Today world's energy systems are facing challenges far greater than the 1970s energy crisis. The uncertainty of our current energy system is due to its dependency on fossil fuels. Climate change brought a rapid change in current energy source which is very challenging and unprecedent that requires trillion dollars of investment. Climate change and the effects of depletion are two major challenges would require action to avoid economic and environmental calamity. Such actions need infrastructural changes. The energy dilemma will become more critical to our future, but yet there is a little proof that it is taken seriously. One of alternative energy source would be Solar Energy.

1.1.2 Solar Energy

Solar energy is the energy that comes from solar radiation. The solar radiation produces heat, causes chemical reactions, or generates electricity. Today the energy necessity of the world can be fulfilled by total amount of solar energy incident on Earth. This energy source has the potential to satisfy all future energy needs. Solar energy is a renewable source as it has the ongoing free energy. It produces no greenhouse gases, that is why it is not harmful for our climate. Toady the energy sources create centralization in the world as powerful countries hold the energy sources. But solar energy decentralizes this syndicate. It can go on or off the grid. It will create many new jobs and employments. It

will save our eco-system and livelihood. So far, we get that solar energy will be the best alternative sources for the current energy crisis of the world.

1.1.3 Metamaterial

Metamaterials are engineered structures which may have some unusual electromagnetic properties like, negative permittivity, negative permeability or negative refractive index, inverted Snell's law etc. These properties depend on the design of its individual atoms. Properties are derived from their physical structure, not from their chemistry.

1.1.4 Application of Metamaterial

- Antenna Design
- Invisibility Cloak Design
- Filter Design
- Waveguide Design
- Absorber Design
- Energy harvesting
- Sensing as Sensor
- Solar Cell Design
- SAR Reduction
- Wireless Power Transfer

1.1.5 Metamaterial Absorber to Utilize Solar Energy

Metamaterials are artificial materials. They are not found in nature usually. They have extraordinary electromagnetic properties. These properties can be utilised for making efficient solar absorbers. We know that the absorbance of normal absorber is very low. This low efficiency can be removed by using metamaterial for solar absorbers. Metamaterial solar absorbers are far more efficient than normal absorbers. There are many works related to metamaterial absorbers. In this report, we are also working for a such kind of perfect metamaterial absorber.

1.2 Literature Review

Metamaterial designs and uses have picked up for the need of passionate research, because metamaterials have various extraordinary electromagnetic properties [8]. Actually, Metamaterials are widely considered for numerous applications. V. Veselago

devotee Smith et al. found an artificial metamaterial with negative permeability and permittivity which shows double negative properties [9], [10]. These properties of metamaterials qualify them to be applied as waveguides [11], antennas [12], invisible cloaks [13], filters [14], absorbers [15], [16], detectors [17], specific absorption rates (SAR) [18], [19], super lenses [20], RF lenses [21], polarization converter [22], imaging [23], and various kind of sensors [24]-[27]. These properties and their applications have been studied theoretically as well as practically, since the first verification of metamaterial absorbers (MMA) by Landy et al. in 2008 [28]. In the same year, the demonstration of a single and Tera Hertz MMA at 1.3 THz by Tao et al. opened the door for Tera Hertz applications [29]. Tera Hertz metamaterials are categorized by single band [30], dual-band [31]-[33], triple band [34], multi-band [35]-[37], tunable [38], [39], broadband [40], [41]. Generally, a three-layered like metal-dielectric-metal (resonator) structure is supposed to be a broadband near perfect MMA in solar spectrum. Metal layers prevent the transmission of the electromagnetic (EM) waves, and the dielectric layer helps the structure to create a coupling capacitance is created between the metal and the resonator layer in the structure with the help of dielectric layer [42]-[44]. However, there are other reasons too for a near perfect MMA. Plasmonic resonance characteristics of the dielectric layer [45], [46], perfect impedance match of the metal with the free space of the solar spectrum [47], [48], a symmetric structure of the resonator with good lockup of the electromagnetic waves [49], [50], and a good E-field, H-field and surface charge distribution are also cause for high absorption [51], [52]. Most common MMA absorber structures are three-layered structures, but there also two-layered [53], four-layered [54], [55], multi-layered stacks [56]-[58]. High absorption characteristics are displayed with a wide wavelength even though the structures are ultrathin [59]-[61], because of the periodic structure of artificial design metamaterial absorbers. Lee et al. first discussed about broadband MMA in 2012 with FR4 and copper in the Giga Hertz frequency region [62]. After that, broadband MMA was also disclosed in optical region by many types of research works until today. Some of them are given below with the results the studies found, the materials they used, and their angular and polarization stability.

There are various works regarding to Perfect Metamaterial Absorbers. The outline, manufacture, and characterization of a dual-band metamaterial absorber are displayed by Tao et al. [63]. They have found absorption peaks of 85% at 1.4 THz and 94% at 3.0

THz. Moreover, they showed [64] a metamaterial absorber that works as a strong resonant absorber at THz frequencies. However, their design structure shows outcomes of the absorption are illustrated at 1.3 THz as 70%. A substrate of 1150 × 1150 nm2 with the thickness of 200 nm was suggested by Ahmed M. Montaser [65] for visible frequency range. The high absorption of the structure was 99.46% at 265.8 THz and 99.4% at 556.4 THz. A square shaped resonator with hole setup PMA was proposed by Dincer et al. where the highest absorptivity rate is 99.92% which is achieved at 0.865 THz [66]. But they got 4.56% fractional bandwidth that indicates the quality of proposed perfect metamaterial absorber (PMA). Hu et al. [67] figured out a metamaterial that works in the THz band and having four narrowband high absorptivity of 98, 97, 98, and 97% at frequencies of 0.68, 1.27, 2.21, and 3.05 THz respectively. A metamaterial absorber unit cell structure with 500 × 500 nm^2 dimensions was recommended by Ustunsoy et al. which has 99.99% absorptivity rate at 558.75 Tera Hertz and 99% absorptivity rate at 216.75 Tera Hertz [3]. A compact and dual band tuneable metamaterial absorber based on strontium titanate (STO) crystal substrate was introduced by Li et al. That design structure displayed a maximum absorptivity rate of 97.97% at 0.15 THz, and 95.92% at 0.30 THz [68]. Mulla et al. offered an MMA for solar energy harvesting. The absorptivity rate of absorber has 98.2% at 445.85 Tera Hertz and 99.4% between 624 and 658.3 Tera Hertz. They used Aluminium (Al) as metallic parts of the design structure and the silicon dioxide (SiO_2) is a dielectric material of the structure [69]. Transverse Electric and Transverse Magnetic polarization in both the visible and near infrared (NIR) regions of an Al-GaAs-Al layered multi circular PMA with three near unit absorption peaks high [70]. A nano-composite (SiO_2/Gold) based plasmonic metamaterial which is four layered and polarization independent shows above 85% absorptivity from the 400nm to the 750nm wavelength [71]. A three-layered MMA consists of TiN-SiO_2-TiN shows an average absorption over 95% for the full visible range at TE and TM mode. TiN (Titanium Nitride) was used as a refractory plasmonic component [72]. A new three-layered MMA was suggested by C. Tun et al. where a phase-change material ($Ge_2Sb_2Te_5$) layer is used along with gold as a metal for near infra-red and the visible wavelength. They got two-peak absorption at 96.8% at 610 nm and 96.2% at 870 nm [73]. A meta nano-pillar array consists of Gold/Silicon (Au/Si) was used by S. Cao et al. to get an average 96% absorptivity rate for the whole visible wavelength range where 60º angular stability is applied for both transverse electric (TE) and transverse magnetic (TM) polarization [74]. A Silicon based MMA with Gold (Au) as a metal and SiO2 as a

dielectric layer as used for high absorption which speciality was conical and circular holes in the structure had absorptivity above 80% from 437.9 nm to 578.3 nm. The highest peak got 98.2% absorption where the angular stability was set up to 60º [75]. A metal-dielectric-metal layered meta material absorber based on a meta surface formatting got 92% absorptivity in the optical wavelength and also gained an average of 83% absorptivity rate [76]. Silicon and Nickel based absorbers can be implemented with over 90% absorption for the visible wavelength and over 99% from 500 nm to 560 nm [77]. Gold, Silicon Dioxide and Gold (Au-SiO_2-Au) layered Genetic Algorithm (GA) based absorber had over 90% absorption and 40º angular stability for transverse electric (TE) and transverse magnetic (TM) polarizations [78]. An MMA with normal quartz substrate with two gold layers had more than 80% absorption from 575 nm to 760 nm and it got four near unity peaks [79]. Metamaterial absorbers also can be found in lower MIR [80], IR [81], UV [82], Hz [83], kHz [84], MHz [85], GHz [86], THz [87], [88] with visible region as discussed above with applications like STPV [89], [90], cryptography [91], thermal detector [92], light trapper [93], sound absorption [94], detectors [95], underwater sound absorption [96], photonic circuit [97], military radar devices [98], detection of explosives [99], filter [100], reflector [101], refractive index sensor [102], thermal imaging [103], antenna [104], energy harvesting [105], [106], light detection [107], [108], imaging [109], [110], sensors [111]-[114].

1.3 Research Goal

In this report, our designed absorber shows double negativity at visible frequency range. Our design is inspired by many previous works with various applications related to metamaterial. If the thickness of metal and substrate, the polarization angle of design structure, resonator's radius, and resonator's shape are varied by some parameters, the absorbance of the absorber will also change.

Considering earlier literature review, the objectives of our research are –

- To find an average absorbance above 90%.
- To get several peak absorbance around 99%.
- To improve the absorbance at visible frequency range because it very important for solar harvesting.
- To design a very simple and flexible structure so that it can be easily possible for industrial implementation.
- To design a structure which works as a multiband absorber.

- To use industrially available materials for the design so that it would be easy to produce industrially.

The development of proposed structure would open new scope of possibilities for more effective photovoltaic solar cells. The research in metamaterial fields is gradually growing. Continuous research of these forms of MMAs will open up a new age with specific implementations for the relevant sector.

1.4 Organization of the report

- **Chapter 1 Introduction:** In this chapter, the solar energy and current world's energy perspective is described. Also, chronological previous works related to metamaterial absorber are mentioned. There is also short description on research goal.
- **Chapter 2 Design & Simulation:** In this chapter, the design steps are described elaborately. The substrate and resonator design along with their parameters are stated. Choice of proper boundary condition and simulation setup are explained in brief.
- **Chapter 3 Result Analysis:** Enormous parametric inspections have been carried out for proper characterization of the PMA absorber. Individual peak analysis from Scattering parameter is done. Effective medium properties are examined. Farfield and mesh view of the model is stated also. In added to that a simple power analysis is done.
- **Chapter 4 Comparative Study:** This chapter contains diverse comparison of this model about different polarization angles, transverse electric and transvers magnetic mode.
- **Chapter 5 Conclusion:** The chapter depicts a brief summary of the work done and also shows the feasibility of future works.

CHAPTER 2
DESIGN & SIMULATION

2.1 Introduction

This research work is based on CST Studio simulation. This kind of nano scale metamaterial research has not implemented practically till now. To simulate our proposed design in CST, some procedures have been followed. In this chapter, material selection, design and simulation process are discussed elaborately.

2.2 Choice of Material

We have to choose metal and dielectric layers which are stable in high temperature and possess perfect optical properties, because the proposed metamaterial structure operates in the optical wavelength. There are various kinds of materials that can be used to create the desired structure model. We have observed the properties of different materials and found out that Aluminium and Gallium Arsenide suited best for our desired result. So, our structure will be Al-GaAs-Al three layered structure.

2.2.1 Aluminium

The optical properties of metallic aluminium are among the most widely measured and analysed of any material [115]. Ellipsometric measurements yield the optical constants directly, but reflectance measurements at normal incidence must be analysed by using dispersion theory. This has recently been done over a wide spectral range for the room temperature UHV reflectance measurements by Shiles et al. [115], who used a self-consistent Kramers-Kronig analysis. The reflectance for smooth unoxidized films at normal incidence as calculated from the results of Shiles et al. [115] by using the Fresnel relation,

$$R(\omega) = \frac{[n(\omega)-1]^2 + k^2(\omega)}{[n(\omega)+1]^2 + k^2(\omega)} \quad (1)$$

Raw aluminium metal and its scanning transmission electron microscopic annular dark-field imaging has been shown in **Fig. 2.1** and the properties are listed in **Table 2.1.**

Fig. 2.1 (a) Raw Aluminium Metal [116]

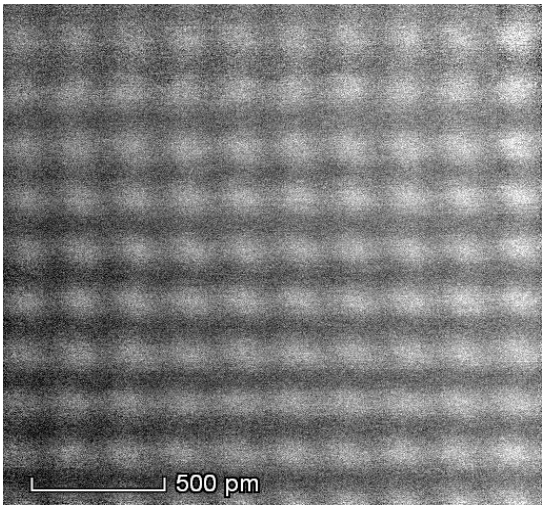

Fig. (b) High-resolution STEM-HAADF micrograph of Aluminium atoms [117]

Table 2.1 Properties of Aluminium (lossy) from CST Library

component1: solid2 & solid3	
Material	Aluminium (lossy)
Type	Lossy metal
Mu	1
Electric condition	$3.56e^{+07}$ [S/m]
Rho	2700 [kg/m^3]
Thermal condition	237 [W/K/m]
Heat capacity	0.9 [kJ/K/kg]
Diffusivity	9.75309e-05 [m^2/s]
Young's modulus	69 [kN/mm^2]
Poisson's ratio	0.33
Thermal expansion	23 [$1e^{-6}/K$]

2.2.2 Gallium Arsenide

Among compound semiconductors Gallium Arsenide (GaAs) is very commonly used one. It contains two elements. One of them is Gallium which is produced as a by-product while smelting metals i.e. Aluminium & Zinc. Now-a-days the use of Gallium Arsenide in solar harvesting has been significantly growing in a drastic manner. It has some other uses also in other optoelectronic devices i.e., light-emitting diodes, lasers. “GaAs is

especially suitable for use in multijunction and high-efficiency solar cells for several reasons:

1. The GaAs band gap is 1.43 eV, nearly ideal for single-junction solar cells.
2. GaAs has an absorptivity so high it requires a cell only a few microns thick to absorb sunlight. (Crystalline silicon requires a layer 100 microns or more in thickness.)
3. Unlike silicon cells, GaAs cells are relatively insensitive to heat. (Cell temperatures can often be quite high, especially in concentrator applications.)
4. Alloys made from GaAs using aluminium, phosphorus, antimony, or indium have characteristics complementary to those of gallium arsenide, allowing great flexibility in cell design.
5. GaAs is very resistant to radiation damage. This, along with its high efficiency, makes GaAs very desirable for space applications.

One of the greatest advantages of gallium arsenide and its alloys as PV cell materials is the wide range of design options possible. A cell with a GaAs base can have several layers of slightly different compositions that allow a cell designer to precisely control the generation and collection of electrons and holes. (To accomplish the same thing, silicon cells have been limited to variations in the level of doping.) This degree of control allows cell designers to push efficiencies closer and closer to theoretical levels. For example, one of the most common GaAs cell structures uses a very thin window layer of aluminium gallium arsenide. This thin layer allows electrons and holes to be created close to the electric field at the junction." (Gallium Arsenide - as a Photovoltaic Material, AZO Materials)

A single crystal of having 149.17 grams Gallium Arsenide with 99.9999% purity is shown in **Fig. 2.2** and the optical properties derived from CST Material Library are listed in **Table 2.2.**

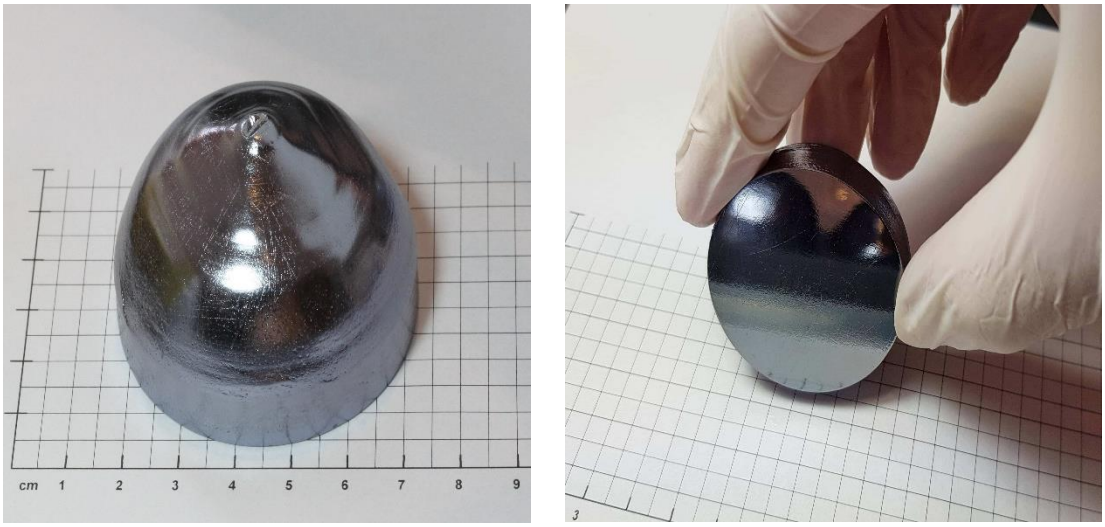

Fig. 2.2 Gallium Arsenide single crystal 149.17 grams 99.9999% purity [118]

Table 2.2 Properties of Gallium Arsenide (lossy) from CST Library

component1: solid1	
Material	Gallium Arsenide (lossy)
Type	Normal
Epsilon	12.94
Mu	1
Electric tand.	0.006 (Const. fit)
Rho	5320 [kg/m^3]
Thermal condition	54 [W/K/m]
Heat capacity	0.33 [kJ/K/kg]
Diffusivity	3.07587e^{-05} [m^2/s]
Young's modulus	85 [kN/mm^2]
Poisson's ratio	0.31
Thermal expansion	5.8 [1e^{-6}/K]

2.3 Design Process

Our proposed model is Al-GaAs-Al three layered sandwiched model. GaAs is the dielectric layer. This GaAs is the substrate of the model. There is an Aluminium resonator in front of the substrate.

2.3.1 Substrate Design

The substrate is made of Gallium Arsenide. Gallium Arsenide is most commonly used efficient semiconductor which is used in many optoelectronic devices. With GaAs substrate, we can apply a wide range of design modules to obtain our desired result. The design and the thickness of the layer is very much crucial for controlling the efficiency of the cell. The proposed model substrate is square shaped. By using square shaped substrate with different thickness, different results can be achieved with different significances. After several attempts, the best absorption rate is found at 566×566 nm^2 size and 260 nm thickness.

2.3.2 Resonator Design

Designing the Aluminium resonator is another crucial part of this modelling. We know that when a material deals with wavelength greater than its size it shows unusual characteristics and becomes metamaterial. The designed resonator has an octagonal shape and the length of the edge is 186.4 nm. The wavelength range of visible lights are 380 nm to 730 nm [119]. Hence the resonator is designed in such parameter that visible wavelength is greater than its edge. Because of the octagonal shape the resonator became polarization insensitive. The thickness of the resonator is chosen 75 nm and it also has significant effect in the absorption rate. The unit cell and its Left, Top and Right view is shown in **Fig. 2.3, Fig. 2.4, Fig. 2.5** and **Fig. 2.6** respectively.

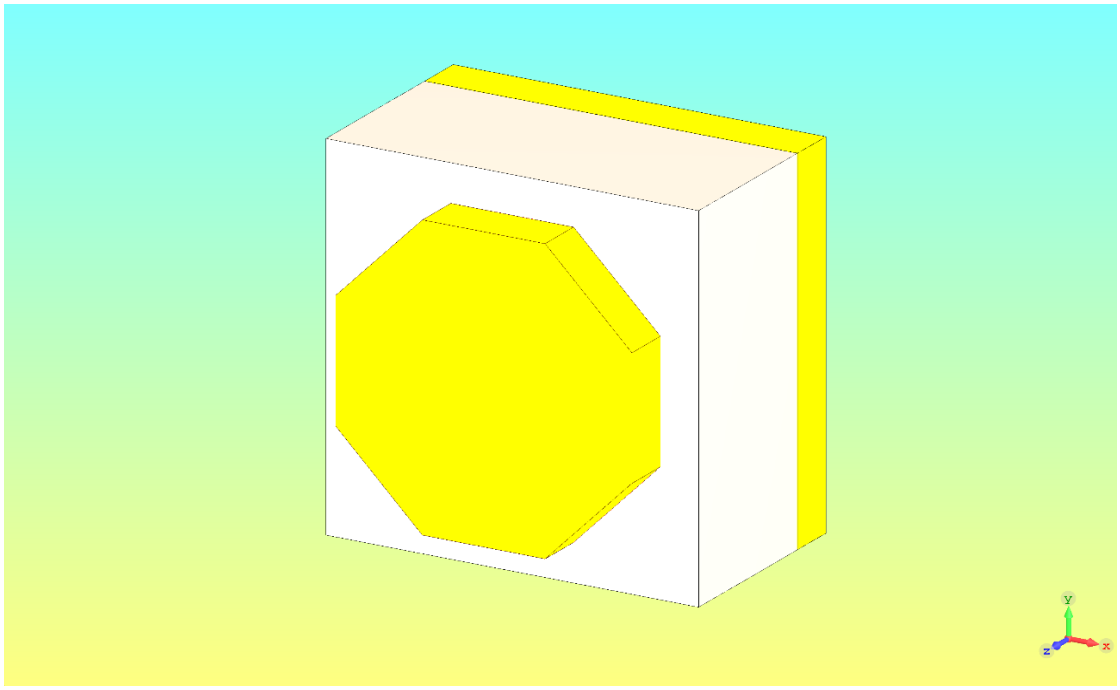

Fig. 2.3 Unit Cell of Designed DNG Metamaterial Absorber

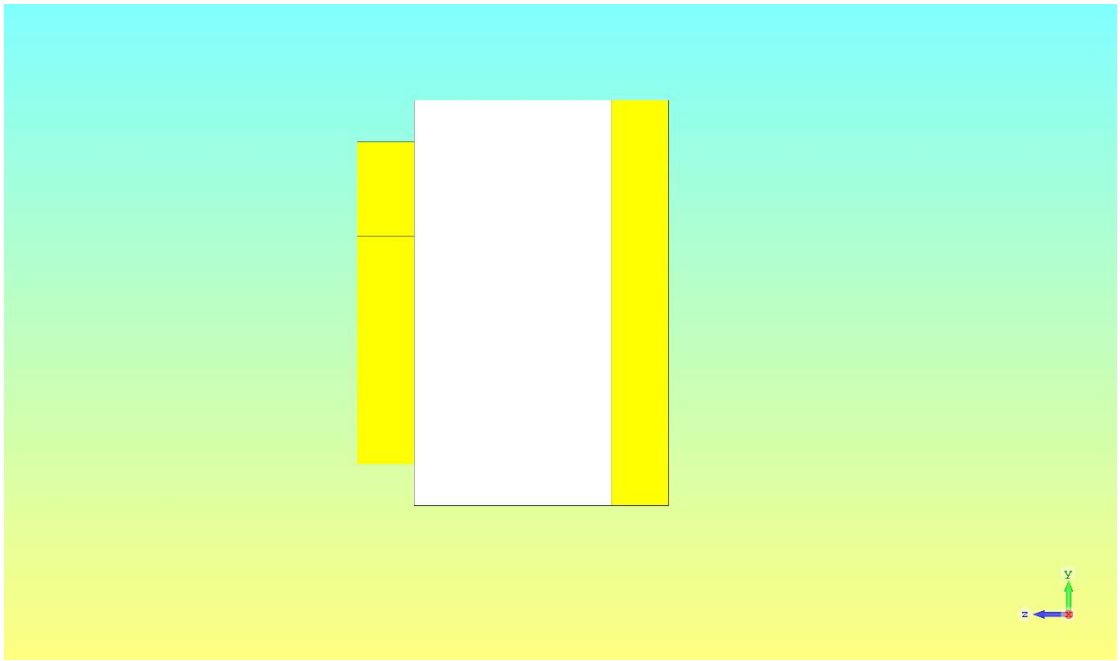

Fig. 2.4 Side Left view of the unit cell

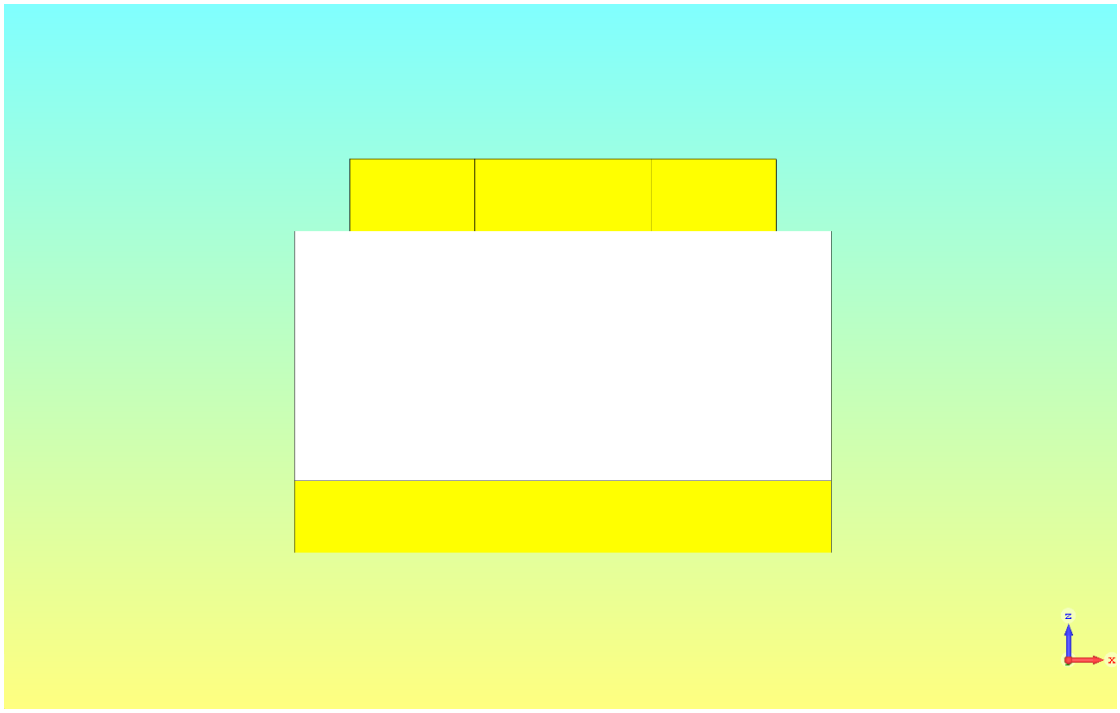

Fig. 2.5 Top view of the unit cell

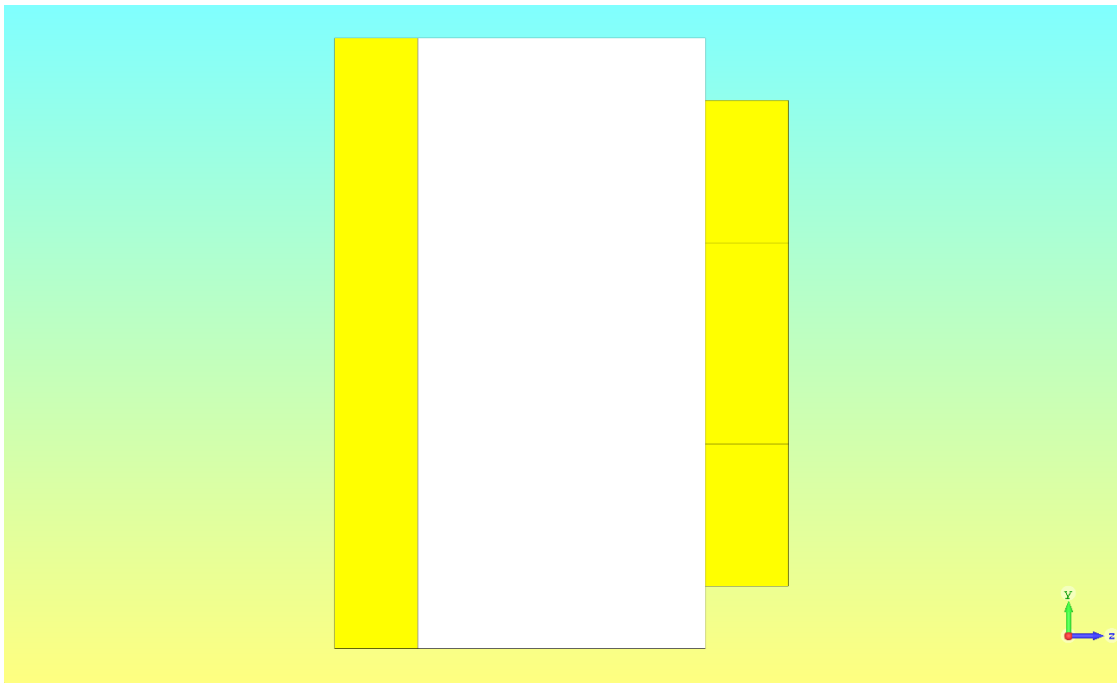

Fig. 2.6 Side Right view of the unit cell

2.3.3 Parameters

The dimensions and all parametric values of our proposed design are depicted in **Fig. 2.7** and tabulated in **Table 2.3.**

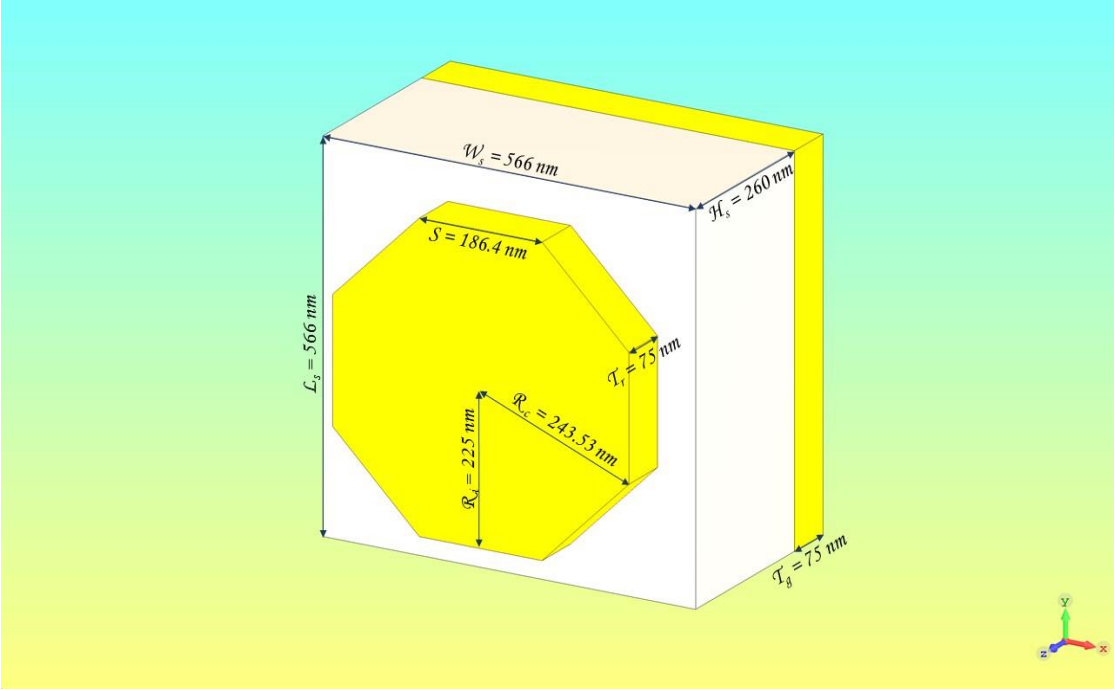

Fig. 2.7 Unit cell with parameters

Table 2.3 Parameters of proposed PMA structure

Substrate	Value (nm)	Resonator	Value (nm)
Substrate Width, W_s	566	Resonator Sidearm, S	186.4
Substrate Length, L_s	566	Resonator Thickness, T_r	75
Substrate Height, H_s	260	Circumcircle Radius, R_c	243.53
Ground Plane Thickness, T_g	75	Incircle Radius, R_i	225

2.3.4 Boundaries

A proper boundary condition to simulate the model is very important because it governs stability of computation along with numerical convergence of the system. Boundary conditions of waveguide for TM, TE and TEM mode have been chosen in such way that the absorber can be implemented to build highly efficient solar cell. The most popular boundary conditions are perfect electric conductor (PEC), perfect magnetic conductor

(PMC) and perfect electromagnetic conductor (PEMC). For the PMC, the magnetic field is asymmetrical and the electric field is symmetrical, and for the PEC the magnetic field is symmetrical and the electric field is asymmetrical. PEMC is a nonreciprocal generalization of PEC & PMC boundary conditions.

PEC : $n \times \mathbf{E} = 0$ and $n.\ \mathbf{B} = 0$

PMC : $n \times H = 0$ and $n.\ \mathbf{D} = 0$

PEMC : $n \times (H + M\mathbf{E}) = 0$ and $n.\ (\mathbf{D} - M\boldsymbol{B}) = 0$

Here, M denotes admittance. PEMC has been chosen as proper boundary condition because it is possible to transform any given PEMC boundary to PEC and PMC boundaries. While analysing tiny scatterers and modelling mixtures that contain PEMC particles embedded in a background medium with PEMC boundary the duality transformation is useful. When a PEMC boundary object is placed in an electromagnetic field, the cross-coupling effect of the boundary condition results in a more complex scattering response than in the case of pure dielectric, PEC, or PMC objects. Once the electromagnetic response of small PEMC spheres is known, it is possible to compute the effective material parameters of a mixture where such spheres (of subwavelength size) are imbedded in neutral dielectric background material [120].

2.4 Simulation

Appropriate setup of simulation and having proper boundary conditions is necessary to achieve desired absorption rate. The absorption rate is obtained from scattering parameter. There are some approaches related to the electromagnetic amounts, boundary conditions supress those approaches. In this design for the transverse electromagnetic (TEM) mode, periodic boundary condition of the perfect electric conductor (PEC) was taken from x-axis and periodic boundary condition of the perfect magnetic conductor (PMC) was taken from y-axis. A waveguide port is initiated in negative z-axis to pass operating wavelength. Open space on both side of z-axis with a perfectly matched layer (PML) is applied to reduce scattering. Linearly polarized planar wide-spectrum wave incidence on the planned absorber's top surface for simulation. Floquet port on z-axis has been used to simulate the model in TM and TE mode with the master and the slave being in the x-axis and the y-axis, respectively. A higher mesh order is used with a view to rendering more precise simulation results. The frequency domain solver in the Computer Simulation Technology Microwave Studio (CST MWS) is used to simulate the model based on the Finite Integration Technique (FIT). It is also possible to use time-domain

solver for simulating such metamaterial absorber models [121]. But the frequency domain solver is more suitable for the proposed design. The two solvers use two different methods to solve the same problem. Both solvers are originally from the FIT (Finite Integration Technique) which works on the Integral Formulation of the Maxwell Equations. Thus, it is pertinent that both solvers give approximately same results. If the model is correct and simulation parameters are properly defined for both solvers, they do give similar results. Frequency domain solvers are useful for smaller structures like unit cells and FSS-Frequency Selective Surface. Floquet analysis can be done using frequency domain solver. Frequency domain solver also takes less time and less memory than other depending upon transient behaviour of the source of excitation and modes. While using time domain in CST waveguide-ports has to be aligned (be parallel to) either X, Y or Z axis. But in frequency domain, the waveguide-port can have arbitrary directions. In time domain, the mesh is created in X, Y and Z axis and tiny blocks look like cubes. Harmonic Equations in differential (or integral) form can be used to analyse those blocks. In frequency domain, FEM (finite element method) is used to break the surface into small triangular objects and integral equations are used in phasor form for those tiny surfaces. That's why the time domain solver is good for wide band structures and the frequency domain is good for curvy structures.

CHAPTER 3
RESULT ANALYSIS

3.1 Introduction

In this chapter, the simulated results are analysed in details. This chapter contains numerical analysis, analysis of s-parameter, absorbance and reflectance, effective medium properties, absorbance peak analysis, electric and magnetic field, power analysis, farfield analysis, mesh view.

3.2 Numerical Analysis

Nicolson–Ross–Weir (NRW) method is used to calculate the complex permittivity and permeability which is discussed in reference [122]. Impedance match is very important for absorbance.

The impedance of the unit cell,

$$Z(\omega) = \left[\frac{\mu_r(\omega).\,\mu_0}{\varepsilon_r(\omega).\,\varepsilon_0}\right]^2 \tag{2}$$

and characteristic impedance $Z_0 = (\mu_0/\varepsilon_r)^{1/2} = 376.73 \approx 377\Omega$. (Evaluated in **Fig. 3.1**)

Here,

μ_0 = Permeability of free space,

ε_0 = Permittivity of free space,

μ_r = Relative permeability and

ε_r = Relative permittivity.

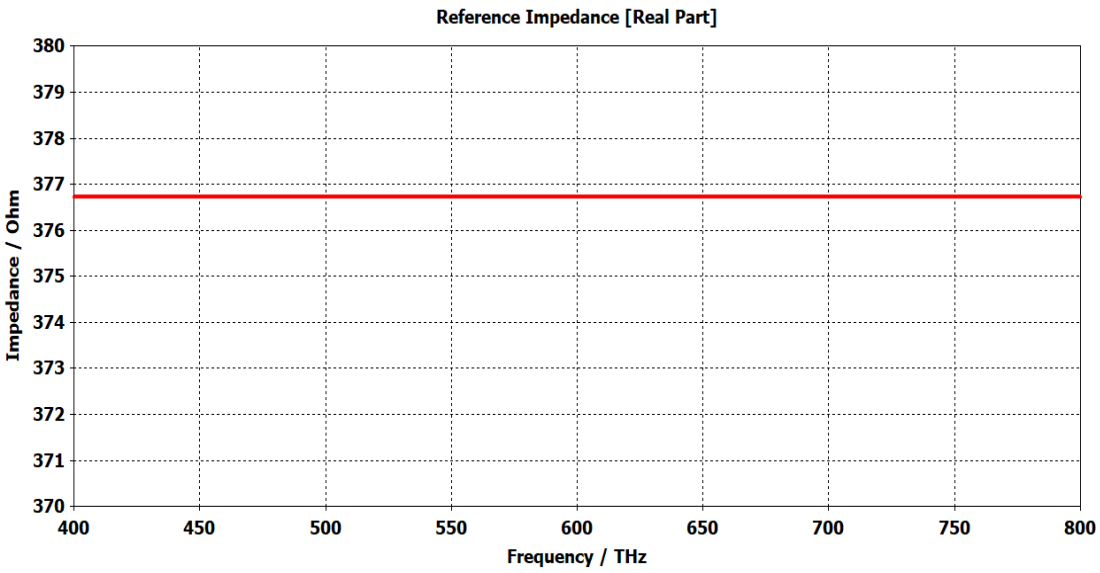

Fig. 3.1 Reference Impedance

Condition $Z(\omega) = Z_0$ can be obtained by measuring the physical dimensions of the design step by step. The design absorption depends on wavelength. That is why design absorptivity will be almost unity at a wavelength. If $Z(\omega) = Z_0$ can be gained, the design will become a super absorber with unity absorption. Although these values are almost equal. The reflection and the transmission coefficients are inversely proportional to absorption, the absorption formula will be,

$$A(\omega) = 1 - R(\omega) - T(\omega)$$
$$= 1 - |S_{11}(\omega)|^2 - |S_{21}(\omega)|^2 \quad (3)$$

Here,

$R(\omega)$ = Linear value of s-parameter S_{11} also called reflection coefficient,

and $T(\omega)$ = Linear value of the S_{21} parameter also called the transmission coefficient. However, transmission coefficient $T(\omega)$ is near zero, because the thickness of aluminium of design blocks all electromagnetic waves.

So, the final absorption formula,

$$A(\omega) = 1 - R(\omega) = 1 - |S_{11}(\omega)|^2 \quad (4)$$

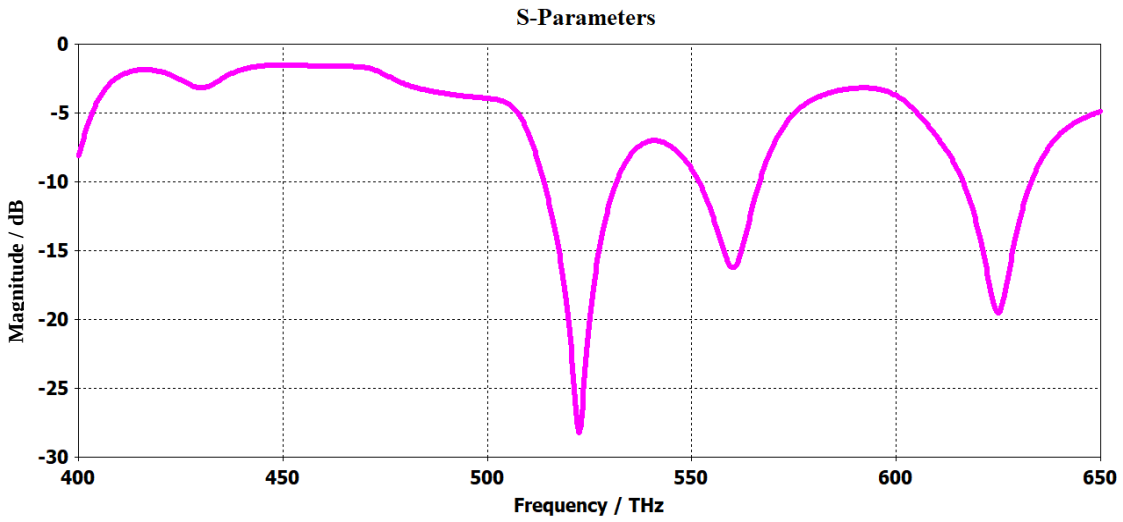

Fig. 3.2 S-Parameter Curve of the Proposed Model

3.3 S-Parameters

The s-parameter is shown in **Fig. 3.2**. For the designed structure, all s-parameters are negative from 400 THz to 800 THz. The maximum negative value is almost -29 dB and the minimum negative value is -1 dB. From this s-parameter curve, it can be proved that the designed structure is a perfect metamaterial absorber.

3.4 Absorbance and Reflectance

From the s-parameter, the absorbance and reflectance can be extracted. The extracted absorbance and reflectance are shown in **Fig. 3.3**. We got best absorption from 430 THz to 580 THz. We got four highest peaks here. Using this design, we got 2 peaks above 99%, one peak above 98% and another peak above 97%. We got first two peaks in DNG region and last two peaks in SNG region. All peaks are above 97%. The highest peak touched almost 100% absorbance. These absorptivity shows that it is a perfect metamaterial absorber.

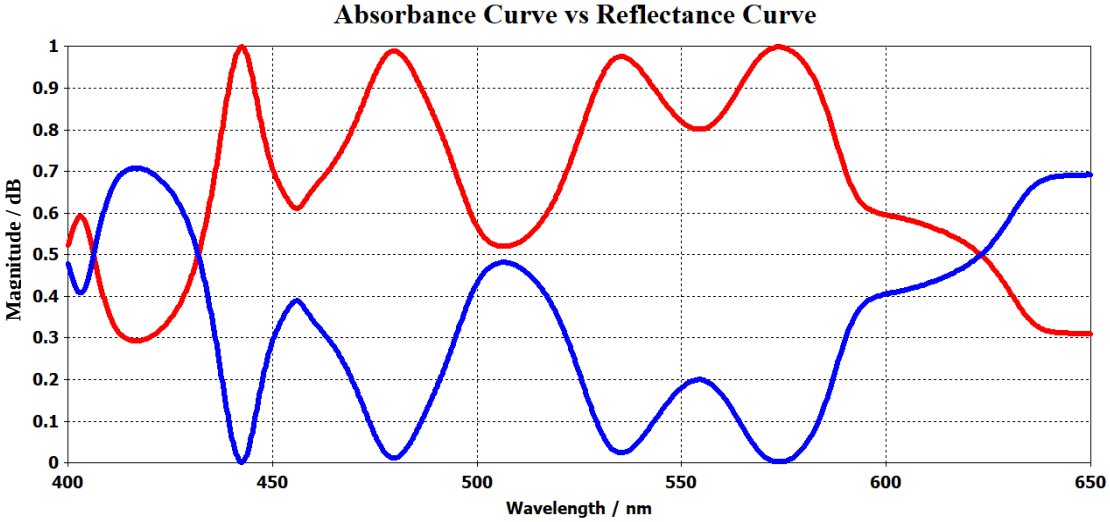

Fig. 3.3 Absorbance and Reflectance curves

3.5 Effective Medium Properties

The electrical and magnetic properties of metamaterial absorber include permittivity, permeability and refractive index. The extracted permittivity, permeability and refractive index along with s-parameters are shown in **Fig. 3.4**. Permittivity, permeability and refractive index all parameters are negative from 400 nm wavelength to 525 nm wavelength. In this region we got two peak absorbance. For these peaks, the designed model became DNG metamaterial. And from the figure, it is seen that permeability and refractive index once became positive, it never became negative. But after slightly becoming positive, permittivity again remains negative till 610 nm wavelength. In this region we got another two peaks and using these peaks the model can be utilized as a SNG. From **Fig. 3.4**, it is appeared that the proposed design has both DNG and SNG properties.

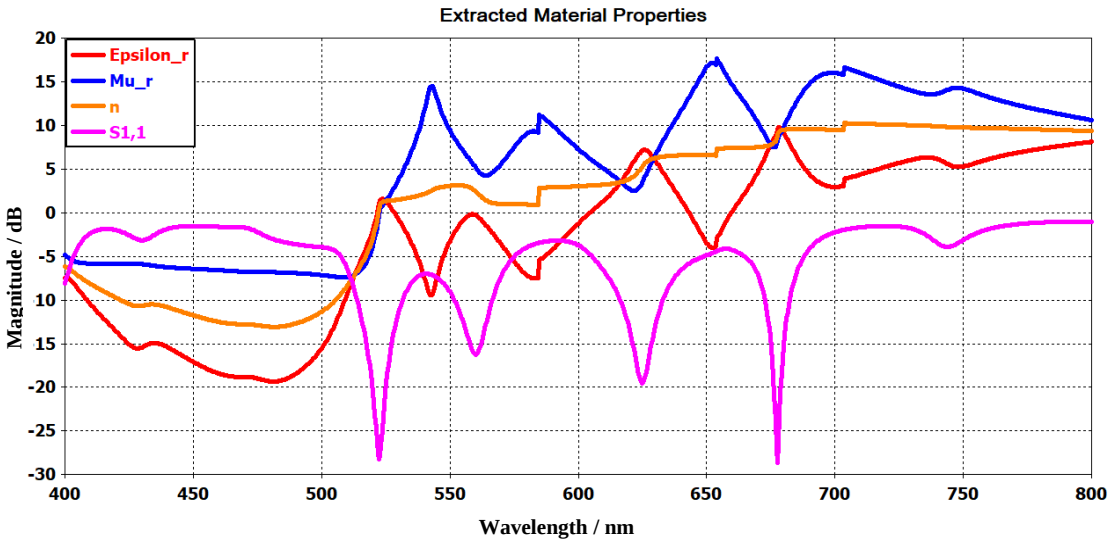

Fig. 3.4 Extracted Material Properties

3.6 Absorbance Peak Analysis

Among many peaks there are four peaks in visible frequency range. The effective medium properties and absorption percentage of peak values in absorption curve within the visible frequency range is tabulated in **Table 3.1** and a closed view of each peak is shown in **Fig. 3.5, Fig. 3.6, Fig. 3.7, Fig. 3.8, Fig. 3.9, Fig. 3.10, Fig. 3.11** and **Fig. 3.12**

Table 3.1 Electric and magnetic properties at peak points

Wavelength nm	Absorbance %	S-Parameter dB	Permittivity, ε_r dB	Permeability, μ_r dB	Refractive Index, n dB
442.43	99.86	-1.67	-15.80	-6.29	-11.05
479.82	98.87	-2.85	-19.30	-6.80	-13.05
535.34	97.61	-7.96	-3.54	7.14	1.80
573.88	99.84	-5.51	-5.00	6.99	0.99

3.6.1 Peak 01 (Maximum)

The maximum peak absorbance of peak 01 of our design is shown in **Fig. 3.5**. In this figure, it is seen that we got 99.86% absorbance at 442.43 nm. This peak is about to near unity absorbance. It can also be seen that this band is narrow band and it has above 90% absorbance from 440 nm to 445 nm.

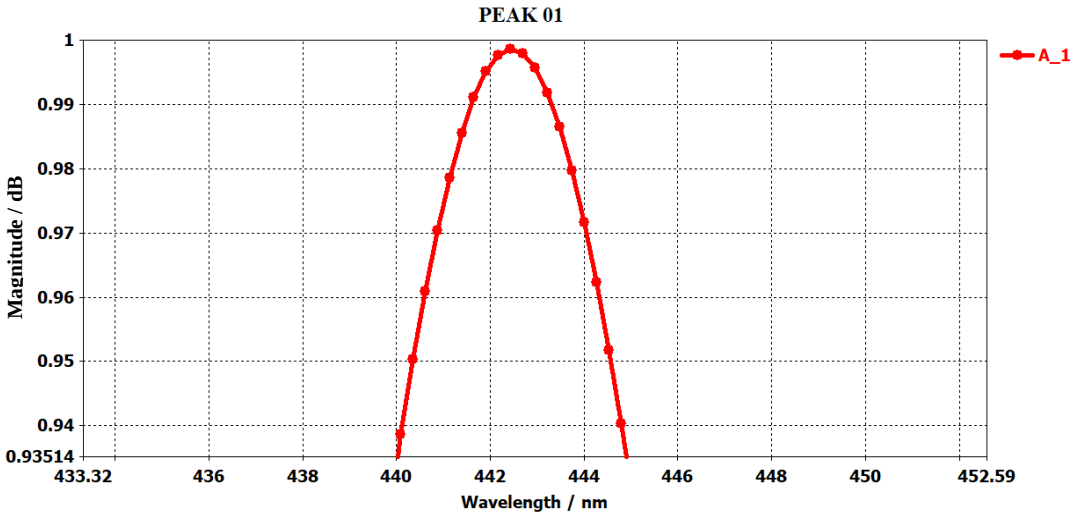

Fig. 3.5 Close View of Absorbance Peak 01

Extracted Material Properties of peak 01 are shown in **Fig. 3.6**. From this figure, the permittivity, permeability, refractive index and s-parameter can be determined. For peak 01, permittivity is -16.8 dB, permeability is -6.29 dB, refractive index is -11.05 dB and s-parameter -1.67 dB are observed. From the value of permittivity and permeability, it can be said that this peak belongs to double negative region.

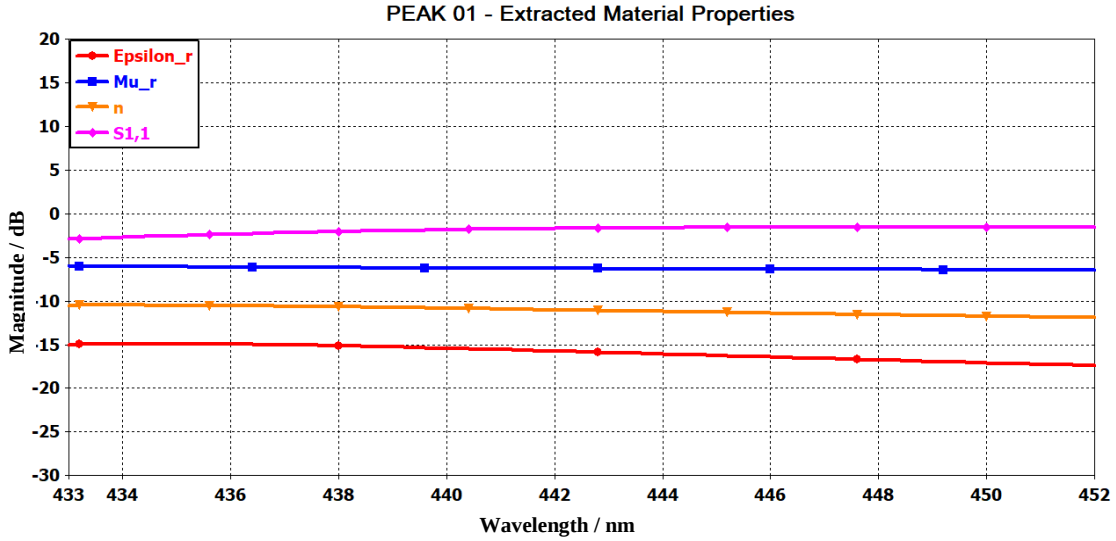

Fig. 3.6 Extracted Material Properties of Peak 01

3.6.2 Peak 02

The peak absorbance of peak 02 of our design is shown in **Fig. 3.7**. In this figure, it is seen that we got 98.87% absorbance at 479.82 nm. This peak is below 99% absorbance. It can also be seen that this band is relatively wide band and it has above 90% absorbance from 475 nm to 485 nm.

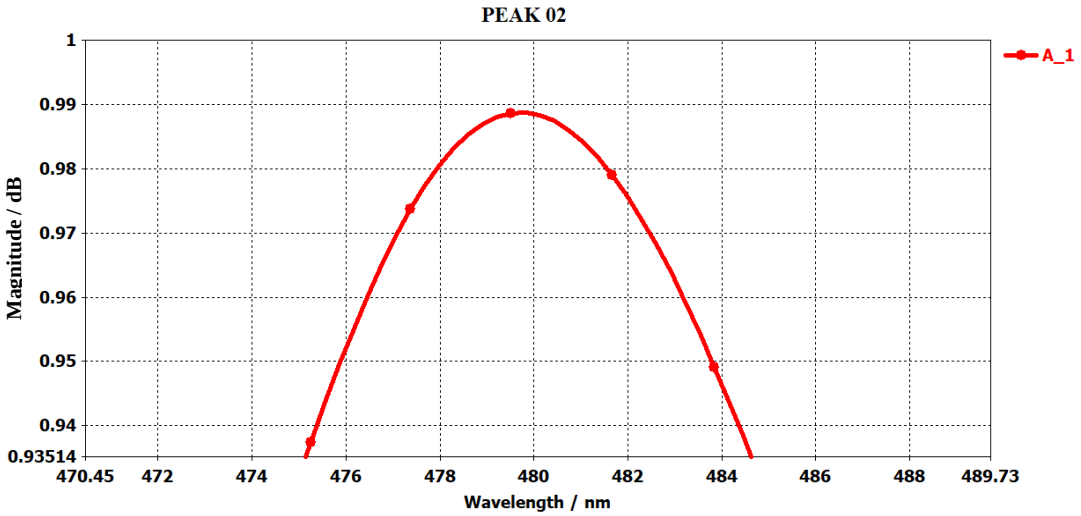

Fig. 3.7 Close View of Absorbance of Peak 02

Extracted Material Properties of peak 02 are shown in **Fig. 3.8**. From this figure, the permittivity, permeability, refractive index and s-parameter can be determined. For peak 02, permittivity is -19.30 dB, permeability is -6.80 dB, refractive index is -13.05 dB and s-parameter -2.85 dB are observed. From the value of permittivity and permeability, it can be said that this peak belongs to double negative region.

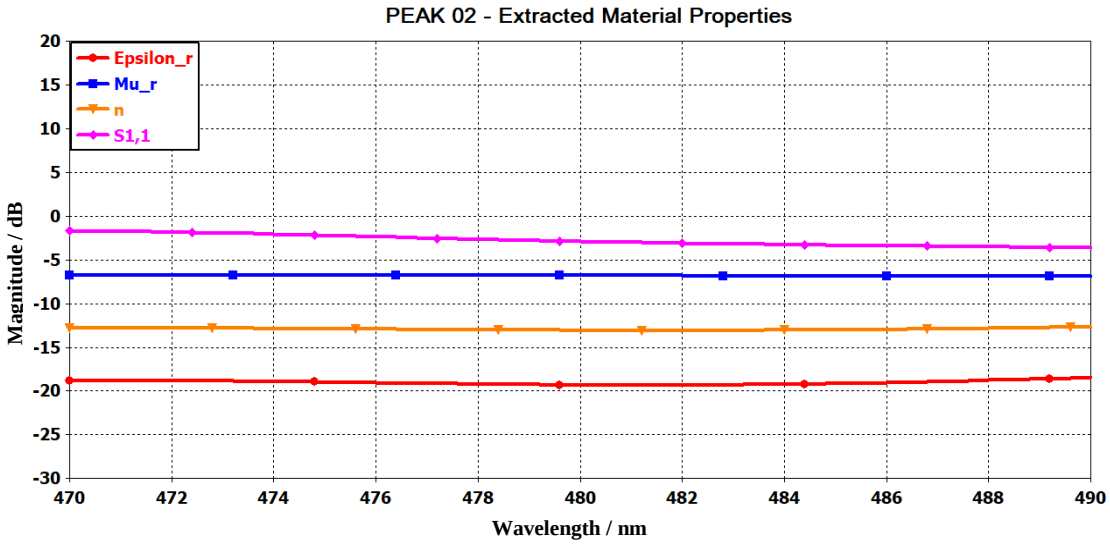

Fig. 3.8 Extracted Material Properties of Peak 02

3.6.3 Peak 03

The peak absorbance of peak 03 of our design is shown in **Fig. 3.9**. In this figure, it is seen that we got 97.61% absorbance at 535.34 nm. This peak is below 98% absorbance. It can also be seen that this band is relatively wide band and it has above 90% absorbance from 530 nm to 542 nm.

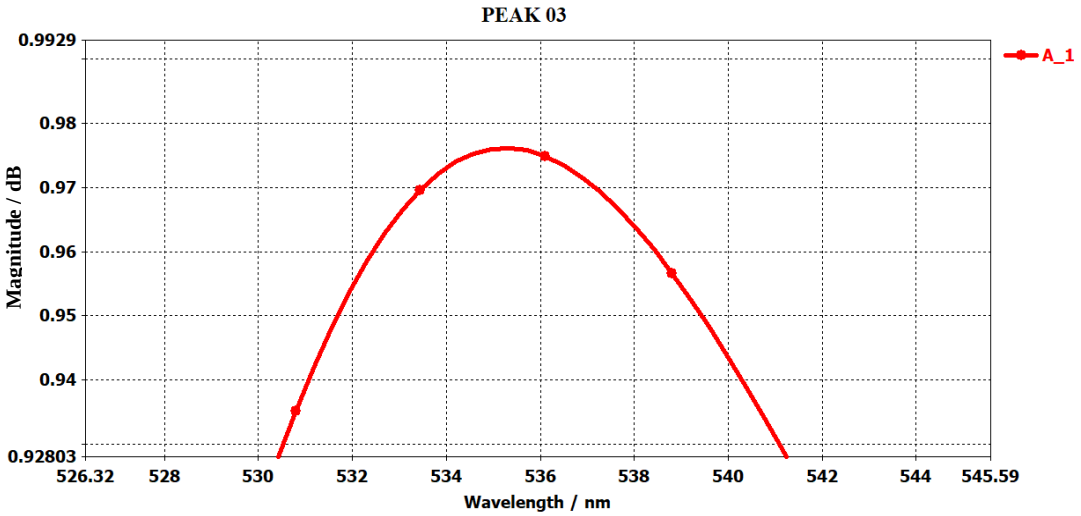

Fig. 3.9 Close View of Absorbance of Peak 03

Extracted Material Properties of peak 03 are shown in **Fig. 3.10**. From this figure, the permittivity, permeability, refractive index and s-parameter can be determined. For peak 03, permittivity is -3.54 dB, permeability is 7.14 dB, refractive index is 1.80 dB and s-parameter -7.96 dB are observed. From the value of permittivity and permeability, it can be said that this peak belongs to single negative region.

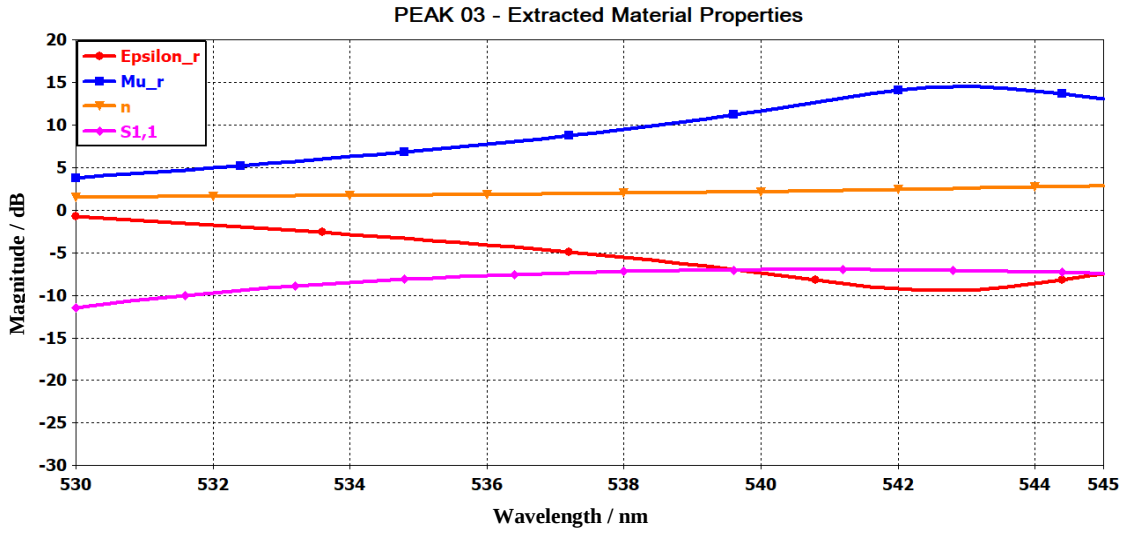

Fig. 3.10 Extracted Material Properties of Peak 03

3.6.4 Peak 04

The peak absorbance of peak 04 of our design is shown in **Fig. 3.11**. In this figure, it is seen that we got 99.84% absorbance at 573.82 nm. This peak is about to near unity absorbance. It can also be seen that this band is wide band and wider than previous three bands, because it has above 90% absorbance from 566 nm to 582 nm.

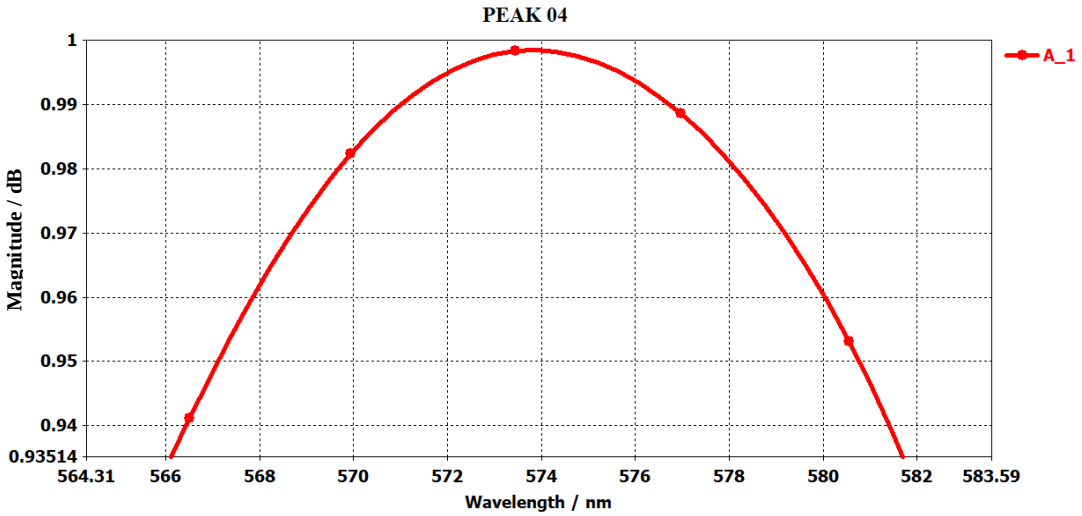

Fig. 3.11 Close View of Absorbance of Peak 04

Extracted Material Properties of peak 04 are shown in **Fig. 3.12**. From this figure, the permittivity, permeability, refractive index and s-parameter can be determined. For peak 02, permittivity is -5 dB, permeability is 6.99 dB, refractive index is 0.99 dB and s-parameter -5.51 dB are observed. From the value of permittivity and permeability, it can be said that this peak belongs to single negative region.

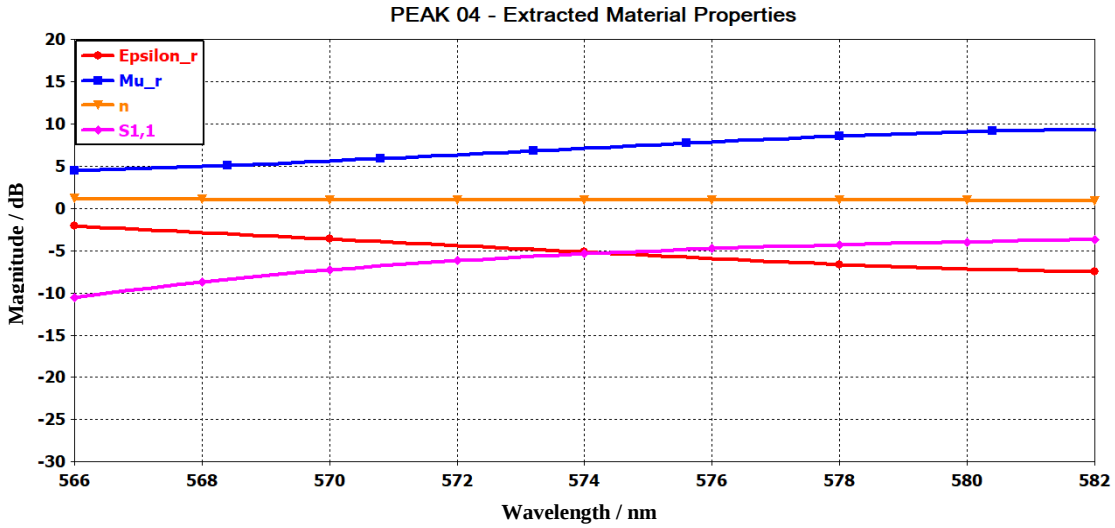

Fig. 3.12 Extracted Material Properties of Peak 04

3.7 Electric and Magnetic Field

In this section, Electric and Magnetic Fields of designed model are analysed. We got four best peak absorbance in four specific frequency.

Fig. 3.13 reveals a deep TEM E-field and magnetic field with first distinct wavelength. This is one of the main reasons for previously discussed higher absorption. The e-field is clearly strongly confined to the dielectric GaAs layer, which stimulates the electrical dipolar resonance moment that is visible in **Fig. 3.13**. In the centre of structure, the electrical field is primarily dispersed. High points of the e-field are primarily observed on the metal resonator/dielectric surface, which indicate plasmon effect of the surface. These plasmons on the surface provided the ideal dipole for the magnification of E-field.

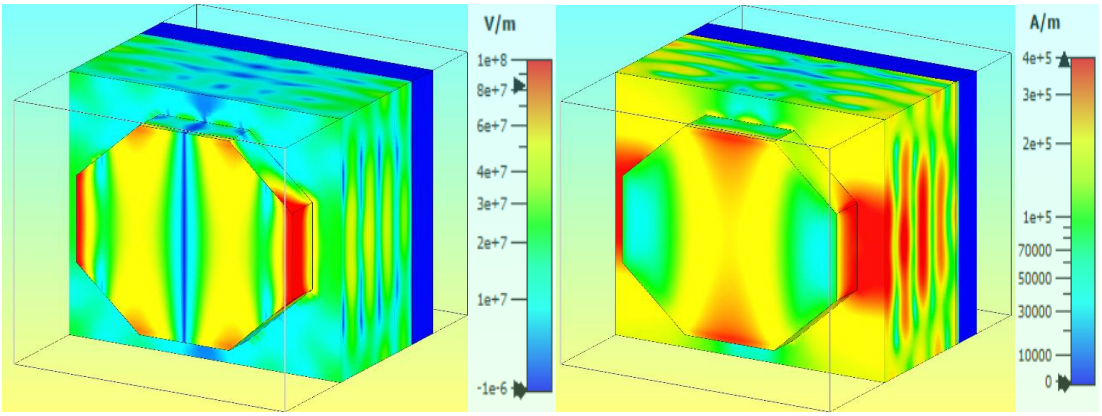

Fig. 3.13 Electric and Magnetic Fields of Peak 01

Fig. 3.14 demonstrated magnetic field for second wavelength in TEM mode as like as E-field. As stable and dispersed e-field, the structure has an extremely good H-field distribution that leads to good MMA for the optical area as a result of the structure. Metal magnetic field is strongly located on metal resonator and is enclosed by the dielectric layer shown in figure.

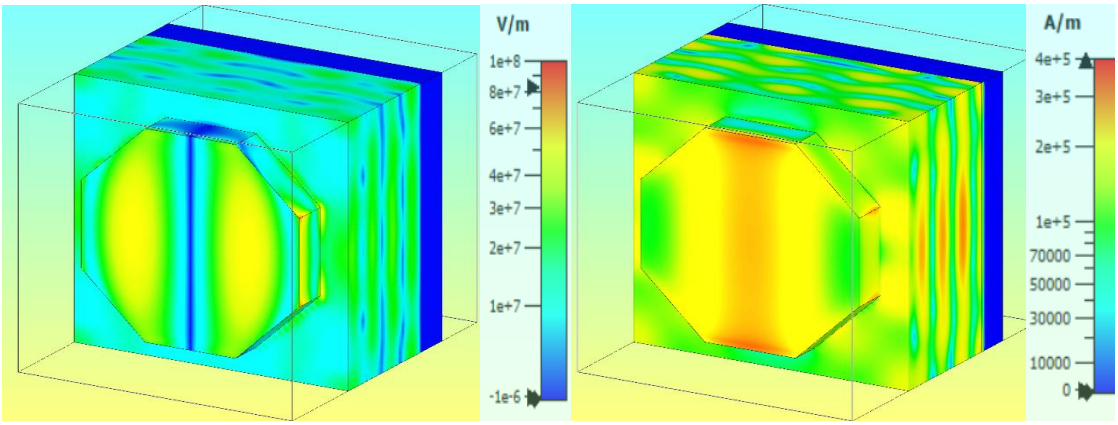

Fig. 3.14 Electric and Magnetic Fields of Peak 02

Fig. 3.15 show that the intensity of the magnetic field is strong in the centre of the structure. The H-field changes direction only when the polarization mode is TEM. A Loop from metal layer to metal resonator produces a loop against parallel current density. The current density that is closely connected with the H-field increases the artificial magnetic dipolar moment.

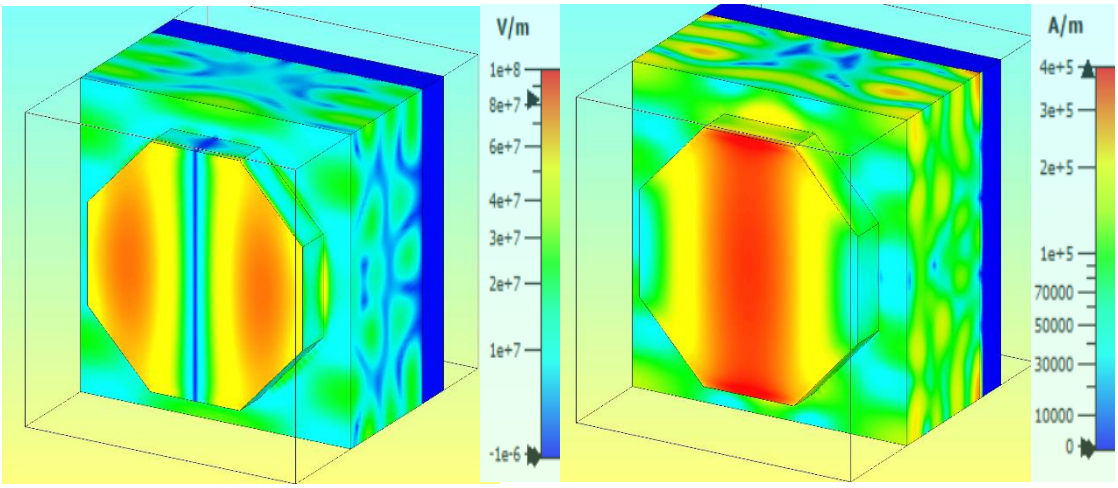

Fig. 3.15 Electric and Magnetic Fields of Peak 03

An important factor for effective absorption over a large bandwidth is the good surface charge distribution with high E-field and H-field. Surface Charge Distribution is demonstrated **Fig. 3.16** for the TEM mode. The figure shows that the surface charge is widely scattered over the entire cell unit. The uniform distribution of the circulating surface charge is the cause of the strong electromagnetic field produced by the structure described above in the dielectric layer.

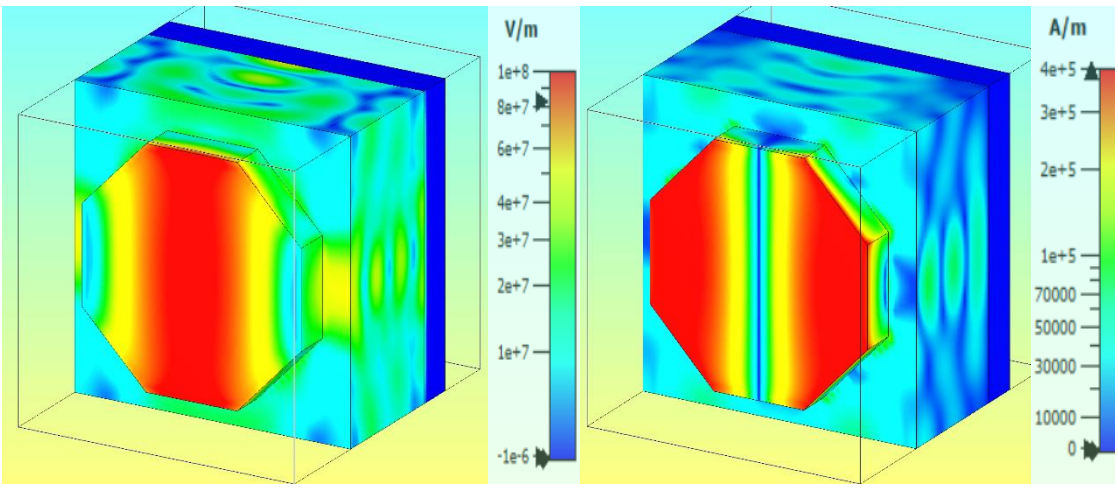

Fig. 3.16 Electric and Magnetic Fields of Peak 04

CHAPTER 4
COMPARATIVE STUDY

4.1 Introduction

This chapter describes comparative analysis of different results. This analysis is made based on polarization angle, TM, TE and TEM mode, and relative comparison of material and shape.

4.2 Polarization Angle

Another advantage of the proposed model is that it is fully independent of polarization angle. Results in various polarization angle and in terms of maximum absorption peaks in TEM mode are compared in **Table 4.1**.

Table 4.1 Polarization Insensitivity of the model.

Polarization Angle	Maximum Absorption Peaks
0°	**99.86% at 442.43**
	98.87% at 479.82
	97.61% at 535.34
	99.84% at 573.88
30°	**99.87% at 442.43**
	98.84% at 479.82
	97.91% at 534.58
	99.92% at 573.88
60°	**99.87% at 442.43**
	98.84% at 479.82
	97.91% at 534.58
	99.92% at 573.88
90°	**99.90% at 442.43**
	98.70% at 479.51
	98.20% at 534.58
	99.93% at 573.44

4.3 Previous Works

A comparative study with previous works on nano-structured metamaterial absorbers have been illustrated on **Table 4.2**

Table 4.2 Comparison with previous works

Author ⇨ / Topic ⇩	Mulla et al. [2]	Ustunsoy et al. [3]	Li et al. [22]	Bağmancı et al.	Hossain et al [7]	Proposed Model
Design structure	Brick shape	Square shape	Square shape	Cross shape	Hexagonal shape	Octagonal shape
Absorption peaks	1	2	2	1	2	4
Dimension	420 × 155 nm^2	500 × 500 nm^2	40 × 6 μm^2	500 × 500 nm^2	566 × 566 nm^2	566 × 566 nm^2
Range	350–455 THz	0–600 THz	0.1–0.5 THz	430–770 THz	430–750 THz	400–800 THz
Rate of Absorption	99.99% at 403.5 THz	99.99% at 568.75 THz	97.97% at 0.15 THz	99% at 216.75 THz	99.96% at 523.84 THz	99.86% at 442.4 THz
						98.87% at 479.8 THz
		99% at 216.8 THz	95.92% at 0.3 THz		99.60% at 674.12 THz	97.61% at 535.3 THz
						99.84% at 573.9 THz
Year of Publication	2015	2016	2016	2017	2018	2021

4.4 TEM, TM and TE Mode

Regardless of waveguide propagation mode results are similar. Added to that the model is polarization insensitive in all three modes. Thus, the model shows much impressive stability by being independent of polarization angle in TEM, TE and TM mode.

4.5 Material and Shape Comparison

The model is built with the focus of having the simplest design which will be possible to implement industrially easily. The materials have been chosen in such way that they are commercially cheap and very available in nature or can be formed easily artificially. Not only that the model has simple design and cheap materials but also it has gained highest absorption peaks compared to similar previous works. It is successful with a large amount of FBW. The octagonal shape plays key role to distribute the electric field in a bi-symmetric way which creates an electric dipole which is responsible for high absorbance.

CHAPTER 5
CONCULSIONS AND FUTURE WORK

5.1 Introduction

Our target was to develop a perfect material absorber which would have more than 90% absorbance. We achieved our goal. These are discussed in previous chapters. This chapter concludes our works. Brief summery and future aspects are mentioned here.

5.2 Conclusions

We have proposed a double negative polarisation insensitive octagonal-shaped design and investigated the absorbance and other aspects of the metamaterial absorber with numerical upshots. The proposed design was simplistic and elemental, and it has 99.86% absorbance in the visible frequency spectra. Thus, by impedance matching, PMA having high absorptivity can be solicitude for reliable autonomous polarisation behaviour compliance. The proposed PMA is also inconsiderate up to 60 degrees to the incidence angle amid the entire working frequency spectrum for the polarization mode of transverse electric and transverse magnetic. It possesses some incredibly significant properties. The proposed model has numerous focal points contrasted with those in writing. In addition, to understand better and adequately visualize the absorptivity, the electric and magnetic field distributions are displayed and appropriately inspected in this report.

Similarly, an equivalent examination went up against the premise of the number of absorption peak, dimension, absorption rate, and published year. PMA executes and estimates the absorbance near round unity with specified variable. The proposed absorber will lead to the implementation of high-efficiency solar cells with polarization insensitivity. The suggested metamaterial absorber is perfect for solar PV or thermo-dynamic systems.

5.3 Future suggestions

Among various types of absorbing elements Perfect Metamaterial Absorbers are very much promising candidates. Specially in solar harvesting metamaterial absorbers can give a huge boost in efficiency. These absorbers can also be used in various civilian and military products in the future including transparent and bendable materials. Tetra Hertz thermal imaging technology can be built by basing on such metamaterial absorber. They have relatively low volume and density along with narrow band response for such applications.

REFERENCES

[1] C. Li, M. Liu, N. G. Pschirer, M. Baumgarten, and K. Mullen, "Polyphenylene-based materials for organic photovoltaics", *Chemical Reviews*, Vol. 110, 6817–6855, 2010.

[2] B. Mulla and C. Sabah, "Perfect metamaterial absorber design for solar cell applications", *Waves Random Complex Media*, Vol. 25, pp. 382–392, 2015.

[3] M. P. Ustunsoy and C. Sabah, "Dual-band high-frequency metamaterial absorber based on patch resonator for solar cell applications and its enhancement with graphene layers", *Journal of Alloys and Compounds*, Vol. 687, pp. 514–520, 2016.

[4] S. S. Islam, M. R. I. Faruque, and M. T. Islam, "An object-independent ENZ metamaterial-based wideband electromagnetic cloak", *Scientific Reports*, Vol. 6, pp. 33624, 2016.

[5] J. B. Pendry, "Negative refraction makes a perfect lens", *Physical Review Letters*, Vol. 85, pp. 3966, 2000.

[6] M. J. Hossain, M. R. I. Faruque, M. T. Islam, and K. B. Mat, "A New Compact Octagonal Shape Perfect Metamaterial Absorber for Microwave Applications", *Applied Sciences*, Vol. 7, pp. 1263, 2017.

[7] M. J. Hossain, M. R. I. Faruque, and M. T. Islam, "Perfect metamaterial absorber with high fractional bandwidth for solar energy harvesting", *PLOS One*, Vol. 13, no. 11, pp. 0207314, 2018.

[8] C. M. Soukoulis, S. Linden, and M. Wegener, "Negative refractive index at optical wavelengths", *Science*, Vol. 315, pp. 47–49, 2007.

[9] H. Luo and J. Qiu, "Carbon Nanotube/Polyolefin Elastomer Metacomposites with Adjustable Radio-Frequency Negative Permittivity and Negative Permeability", *Advance Electronic Materials*, Vol. 5, no. 6, pp. 1900011, 2019.

[10] D. R. Smith, W. J. Padilla, D. C. Vier, S. C. Nemat-Nasser, and S. Schultz, "Composite medium with simultaneously negative permeability and permittivity", *Phyical Review Letters*, Vol. 84, no. 18, pp. 4184–4187, 2000.

[11] F. Fan et al., "Terahertz transmission and sensing properties of microstructured PMMA tube waveguide," Optics Express, Vol. 23, no. 21, p. 27204, 2015.

[12] M. M. Hasan, M. R. I. Faruque, and M. T. Islam, "Dual band metamaterial antenna for LTE/bluetooth/WiMAX system", *Scientific Reports*, Vol. 8, no. 1, pp. 1–17, 2018.

[13] S. S. Islam, M. R. I. Faruque, and M. T. Islam, "A near zero refractive index metamaterial for electromagnetic invisibility cloaking operation", *Materials (Basel).*, Vol. 8, no. 8, pp. 4790–4804, 2015.

[14] J. Alam, M. R. I. Faruque, and M. T. Islam, "Labyrinth double split open loop resonator based bandpass filter design for S, C and Xband application", *Journal of Physics D: Applied Physics*, Vol. 51, no. 26, 2018.

[15] A. S. Rana, M. Q. Mehmood, H. Jeong, I. Kim, and J. Rho, "Tungsten-based Ultrathin Absorber for Visible Regime", *Scientific Reports*, Vol. 8, no. 1, pp. 2–9, 2018.

[16] S. Yin et al., "High-performance terahertz wave absorbers made of silicon-based metamaterials", *Applied Physics Letters*, Vol. 107, no. 7, 2015.

[17] J. Y. Suen et al., "Multifunctional metamaterial pyroelectric infrared detectors", *Optica*, Vol. 4, no. 2, pp. 276, 2017.

[18] M. I. Hossain, M. R. I. Faruque, and M. T. Islam, "Analysis on the effect of the distances and inclination angles between human head and mobile phone on SAR", *Progress in Biophysics and Molecular Biology*, Vol. 119, no. 2, pp. 103–110, 2015.

[19] M. R. I. Faruque and M. T. Islam, "Design of miniaturized double negative material for specific absorption rate reduction in human head", *PLOS One*, Vol. 9, no. 10, 2014.

[20] X. Zhang and Z. Liu, "Super lenses to overcome the diffraction limit", *Nature Materials*, Vol. 7, no. 6, pp. 435–441, 2008.

[21] D. Schurig, "An aberration-free lens with zero F-number", *New Journal of Physics*, Vol. 10, no. 115034, 2008.

[22] F. Li et al., "Design and implementation of metamaterial polarization converter with the reflection and transmission polarization conversion simultaneously", *Journal of Optics*, Vol. 21, no. 4, pp. 045102, 2019.

[23] J. A. Montoya, Z.-B. Tian, S. Krishna, and W. J. Padilla, "Ultra-thin infrared metamaterial detector for multicolor imaging applications", *Optics Express*, Vol. 25, no. 19, p. 23343, 2017.

[24] G. Duan, J. Schalch, X. Zhao, J. Zhang, R. D. Averitt, and X. Zhang, "An air-spacer terahertz metamaterial perfect absorber for sensing and detection applications", *2017 19th International Conference on Solid-State Sensors, Actuators and Microsystems (TRANSDUCERS)*, Vol. 1, pp. 1999-2002, 2017.

[25] L. Xie, W. Gao, J. Shu, Y. Ying, and J. Kono, "Extraordinary sensitivity enhancement by metasurfaces in terahertz detection of antibiotics", Scientific Reports, Vol. 5, pp. 1–4, 2015.

[26] H. K. Kim, D. Lee, and S. Lim, "A fluidically tunable metasurface absorber for flexible large-scale wireless ethanol sensor applications", *Sensors (Switzerland)*, Vol. 16, no. 8, pp. 1246 2016.

[27] A. Salleh, C. C. Yang, T. Alam, M. S. J. Singh, M. Samsuzzaman, and M. T. Islam, "Development of Microwave Brain Stroke Imaging System using Multiple Antipodal Vivaldi Antennas Based on Raspberry Pi Technology", *Jurnal Kejuruteraan*, Vol. 32, no. 1, pp. 39-49, 2020.

[28] N. I. Landy, S. Sajuyigbe, J. J. Mock, D. R. Smith, and W. J. Padilla, "A Perfect Metamaterial Absorber," *Physical Review Letters*, Vol. 100, no. 20, 2008.

[29] H. Tao, N. I. Landy, C. M. Bingham, X. Zhang, R. D. Averitt, and W. J. Padilla, "A metamaterial absorber for the terahertz regime: design, fabrication and characterization", *Optics Express*, Vol. 16, no. 10, p. 7181, 2008.

[30] N. Liu, M. Mesch, T. Weiss, M. Hentschel, and H. Giessen, "Infrared perfect absorber and its application as plasmonic sensor", *Nano Letters*, Vol. 10, no. 7, pp. 2342–2348, 2010.

[31] Z. H. Jiang, S. Yun, F. Toor, D. H. Werner, and T. S. Mayer, "Conformal dual-band near-perfectly absorbing mid-infrared metamaterial coating", *ACS Nano*, Vol. 5, no. 6, pp. 4641–4647, 2011.

[32] P. Rufangura and C. Sabah, "Dual-band perfect metamaterial absorber for solar cell applications", *Vacuum*, Vol. 120, pp. 68–74, 2015.

[33] Y. Cheng, H. Zhang, X. S. Mao, and R. Gong, “Dual-band plasmonic perfect absorber based on all-metal nanostructure for refractive index sensing application”, *Materials Letters*, Vol. 219, pp. 123-126, 2018.

[34] Y. Cheng, H. Luo, and R. Gong, “Triple narrow-band plasmonic perfect absorber for refractive index sensing applications of optical frequency”, *OSA Contin. 2*, Vol. 2, no. 7, pp. 2113–2122, 2019.

[35] L. Zhao, H. Liu, Z. He, and S. Dong, “Theoretical design of twelve band infrared metamaterial perfect absorber by combining the dipole, quadrupole, and octupole plasmonic resonance modes of four different ring-strip resonators”, *Optics Express*, Vol. 26, no. 10, pp. 12838, 2018.

[36] S. Huang et al., “Metasurface with multi-sized structure for multiband coherent perfect absorption”, *Optics Express*, Vol. 26, no. 6, pp. 7066, 2018.

[37] C. Cao and Y. Cheng, “Quad-Band plasmonic perfect absorber for visible light with a patchwork of silicon nanorod resonators”, *Materials (Basel).*, Vol. 11, no. 10, 2018.

[38] G. Yao, F. Ling, J. Yue, C. Luo, J. Ji, and J. Yao, “Dual-band tunable perfect metamaterial absorber in the THz range”, *Optics Express*, Vol. 24, no. 2, p. 1518, 2016.

[39] H. Li, L. Wang, and X. Zhai, “Tunable graphene-based midinfrared plasmonic wide-angle narrowband perfect absorber”, *Scientific Reports*, Vol. 6, no. 36651, 2016.

[40] Z. Liu, G. Liu, X. Liu, Y. Wang, and G. Fu, “Titanium resonators based ultra-broadband perfect light absorber”, *Optical Materials*, Vol. 83, no. June, pp. 118–123, 2018.

[41] X. Tian and Z. Li, “Visible-near infrared ultra-broadband polarization-independent metamaterial perfect absorber involving phase-change materials”, *Photonics Research*, Vol. 4, no. 4, pp. 146-152, 2016.

[42] J. Wang et al., “Shape-dependent absorption characteristics of three-layered metamaterial absorbers at near-infrared”, *Journal of Applied Physics*, Vol. 074510, no. 2011, 2013.

[43] D. Li, H. Huang, H. Xia, J. Zeng, H. Li, and D. Xie, “Temperature dependent tunable terahertz metamaterial absorber for the application of light modulator”, *Results in Physics*, Vol. 11, no. September, pp. 659–664, 2018.

[44] X. Zhang, Y. Fan, L. Qi, and H. Li, “Broadband plasmonic metamaterial absorber with fish-scale structure at visible frequencies,” *Optical Materials Express*, Vol. 6, no. 7, pp. 2448, 2016.

[45] Y. C. Lai, C. Y. Chen, Y. T. Hung, and C. Y. Chen, “Extending absorption edge through the hybrid resonator-based absorber with wideband and near-perfect absorption in visible region”, *Materials (Basel).*, Vol. 13, no. 6, 2020.

[46] K. Aydin, V. E. Ferry, R. M. Briggs, and H. A. Atwater, “Broadband polarization-independent resonant light absorption using ultrathin plasmonic super absorbers”, *Nature Communications*, Vol. 2, no. 1, pp. 1–7, 2011.

[47] N. Mattiucci, M. J. Bloemer, N. Aközbek, and G. D’aguanno, “Impedance matched thin metamaterials make metals absorbing”, *Scientific Reports*, Vol. 3, pp. 1–11, 2013.

[48] R. Contractor, G. D’Aguanno, and C. Menyuk, “Ultra-broadband, polarization-independent, wide-angle absorption in impedance matched metamaterials with anti-reflective moth-eye surfaces”, *Optical Express*, Vol. 26, no. 18, pp. 24031, 2018.

[49] T. S. Tuan and N. T. Q. Hoa, "Numerical Study of an Efficient Broadband Metamaterial Absorber in Visible Light Region", *IEEE Photonics Journal*, Vol. 11, no. 3, pp. 1–10, 2019.

[50] D. Katrodiya, C. Jani, V. Sorathiya, and S. K. Patel, "Metasurface based broadband solar absorber", *Optical Materials*, Vol. 89, pp. 34–41, 2019.

[51] X. Han, K. He, Z. He, and Z. Zhang, "Tungsten-based highly selective solar absorber using simple nano disk array", *Optics Express*, Vol. 25, no. 24, pp. A1072, 2017.

[52] S. Lee, T. Q. Tran, H. Heo, M. Kim, and S. Kim, "A proposal of a perfect graphene absorber with enhanced design and fabrication tolerance", *Scientific Reports*, Vol. 7, no. 1, pp. 1–10, 2017.

[53] C. Li, H. Fan, Q. Dai, Z. Wei, S. Lan, and H. Liu, "Multipole resonance in arrays of diamond dielectric: A metamaterial perfect absorber in the visible regime", *Nanomaterials*, Vol. 9, no. 9, 2019.

[54] Y. Matsuno and A. Sakurai, "Perfect infrared absorber and emitter based on a large-area metasurface", *Optical Materials Express*, Vol. 7, no. 2, pp. 618, 2017.

[55] X. J. He et al., "Broadband and polarization-insensitive terahertz absorber based on multilayer metamaterials", *Optics Communications*, Vol. 340, pp. 44–49, 2015.

[56] N. T. Q. Hoa, P. D. Tung, P. H. Lam, N. D. Dung, and N. H. Quang, "Numerical Study of an Ultrabroadband, Wide-Angle, Polarization Insensitivity Metamaterial Absorber in the Visible Region", *Journal of Electronic Materials*, Vol. 47, no. 5, pp. 2634–2639, 2018.

[57] H. Lin et al., "A 90-nm-thick graphene metamaterial for strong and extremely broadband absorption of unpolarized light," *Nature Photonics*, Vol. 13, no. 4, pp. 270–276, 2019.

[58] H. Xiong, J. Hong, C. Luo, and L. Zhong, "An ultrathin and broadband metamaterial absorber using multi-layer structures", Vol. 114, no. 6, pp. 064109, 2013.

[59] M. Zhong, "Enhance of the absorption and bandwidth based on an ultra-thin tungsten structure metamaterial absorber in 400-1500 nm range", *Optics & Laser Technology*, Vol. 127, no. February, pp. 106142, 2020.

[60] A. Vora, J. Gwamuri, N. Pala, A. Kulkarni, J. M. Pearce, and D. O. Güney, "Exchanging ohmic losses in metamaterial absorbers with useful optical absorption for photovoltaics", *Scientific Reports*, Vol. 4, pp. 1-13, 2014.

[61] S. Mahmud, S. S. Islam, A. F. Almutairi, and M. T. Islam, "A Wide Incident Angle, Ultrathin, Polarization-Insensitive Metamaterial Absorber for Optical Wavelength Applications," *IEEE Access*, Vol. 8, pp. 129525-129541, 2020.

[62] Y. P. Lee, P. V. Tuong, H. Y. Zheng, J. Y. Rhee, and W. H. Jang, "An application of metamaterials: Perfect absorbers", *Journal of the Korean Physical Society*, Vol. 60, no. 8, pp. 1203–1206, 2012.

[63] H. Tao, C. Bingham, D. Pilon, K. Fan, A. C. Strikwerda, and D. Shrekenhamer et al., "A dual band terahertz metamaterial absorber", *Journal of Physics D: Applied Physics*, Vol. 43, pp. 225102, 2010.

[64] H. Tao, N. I. Landy, C. M. Bingham, X. Zhang, R. D. Averitt, and W. J. Padilla, "Metamaterial absorber for the terahertz regime: design, fabrication and characterization", *Optics Express*, Vol. 16, pp. 7181–7188, 2008.

[65] A. M. Montaser, “Design of Metamaterial Absorber for all bands from Microwave to Terahertz ranges”, *International Journal of Advanced Research in Electronics and Communication Engineering*, Vol. 5, pp. 1475–1481, 2016.

[66] F. Dincer, M. Karaaslan, and C. Sabah, “Design and analysis of perfect metamaterial absorber in GHz and THz frequencies”, *Journal of Electromagnetic Waves and Applications*, Vol. 29, pp. 2492–2500, 2015.

[67] F. Hu, L. Wang, B. Quan, X. Xu, Z. Li, and Z. Wu et al., “Design of a polarization insensitive multiband terahertz metamaterial absorber”, *Journal of Physics D: Applied Physics*, Vol. 46, pp. 195103, 2013.

[68] Z. Li, C. Luo, G. Yao, J. Yue, J. Ji, and J. Yao et al., “Design of a concise and dual-band tuneable metamaterial absorber”, *Chinese Optics Letters*, Vol. 14, pp. 102303, 2016.

[69] B. Mulla and C. Sabah, “Multiband metamaterial absorber design based on plasmonic resonances for solar energy harvesting”, *Plasmonics*, Vol. 11, pp. 1313–1321, 2016.

[70] M. Bağmancı, M. Karaaslan, E. Ünal, O. Akgol, F. Karadağ, and C. Sabah, “Broad-band polarization-independent metamaterial absorber for solar energy harvesting applications”, *Physica E: Low-dimensional Systems and Nanostructures*, Vol. 90, pp. 1–6, 2017.

[71] M. J. Hossain, M. R. I. Faruque, M. R. Ahmed, M. J. Alam, and M. T. Islam, “Polarization-insensitive infrared-visible perfect metamaterial absorber and permittivity sensor”, *Results in Physics.*, Vol. 14, no. 102429, 2019.

[72] M. K. Hedayati et al., “Design of a perfect black absorber at visible frequencies using plasmonic metamaterials”, *Advanced Materials*, Vol. 23, no. 45, pp. 5410–5414, 2011.

[73] W. Li et al., “Refractory Plasmonics with Titanium Nitride: Broadband Metamaterial Absorber,” *Advanced Materials*, Vol. 26, no. 47, pp. 7959–7965, 2014.

[74] C. Wu et al., “Metamaterial-based integrated plasmonic absorber/emitter for solar thermo-photovoltaic systems”, *Journal of Optics*, Vol. 14, no. 2, 2012.

[75] X. Niu et al., “Improved broadband spectral selectivity of absorbers/emitters for solar thermophotovoltaics based on 2D photonic crystal heterostructures”, Journal of the Optical Society of America A, Vol. 35, no. 11, pp. 1832–1838, 2018.

[76] C. Liang et al., “A broadband and polarization-independent metamaterial perfect absorber with monolayer Cr and Ti elliptical disks array”, *Results in Physics*, Vol. 15, no. 102635, 2019.

[77] A. Xomalis, I. Demirtzioglou, Y. Jung, E. Plum, C. Lacava, P. Petropoulos, D. J. Richardson, and N. I. Zheludev, “Cryptography in coherent optical information networks using dissipative metamaterial gates”, *APL Photonics*, Vol. 4, no. 4, pp. 046102, 2019.

[78] H. Bruckl, A. Shoshi, W. Reichi, G. Niessner, and T. Maier, “Wavelength-Selective Metamaterial Absorber for Thermal Detectors”, *AMA Conferences 2015*, pp. 251–256, 2015.

[79] Y. Tang, S. Ren, H. Meng, F. Xin, L. Huang, and T. Chen, “Hybrid acoustic metamaterial as super absorber for broadband low frequency sound”, *Scientific Reports*, Vol. 7, no. 43340, 2017.

[80] K. Shi, G. Jin, R. Liu, T. Ye, and Y. Xue, “Underwater sound absorption performance of acoustic metamaterials with multi-layered locally resonant scatterers”, *Results in Physics*, Vol. 12, pp. 132–142, 2019.

[81] P. V. Tuong, J. W. Park, V. D. Lam, W. H. Jang, S. A. Nikitov, and Y. P. Lee, "Dielectric and Ohmic losses in perfectly absorbing metamaterials", *Optics Communications*, Vol. 295, pp. 17–20, 2013.

[82] N. I. Landy, C. M. Bingham, T. Tyler, N. Jokerst, D. R. Smith, and W. J. Padilla, "Design, theory, and measurement of a polarization insensitive absorber for terahertz imaging", *Physical Review B*, Vol. 79, no. 12, pp. 125104, 2009.

[83] Y. Gong et al., "Highly flexible all-optical metamaterial absorption switching assisted by Kerr-nonlinear effect", *Optics Express*, Vol. 19, no. 11, pp. 10193, 2011.

[84] C. Shao, H. Long, Y. Cheng, and X. Liu, "Low-frequency perfect sound absorption achieved by a modulus-near-zero metamaterial", *Scientific Reports*, Vol. 9, no. 13482, 2019.

[85] L. Zigoneanu, B. I. Popa, A. F. Starr, and S. A. Cummer, "Design and measurements of a broadband two-dimensional acoustic metamaterial with anisotropic effective mass density", *Journal of Applied Physics*, Vol. 109, no. 5, 2011.

[86] W. Zuo, Y. Yang, X. He, D. Zhan and Q. Zhang, "A Miniaturized Metamaterial Absorber for Ultrahigh-Frequency RFID System", *IEEE Antennas and Wireless Propagation Letters*, Vol. 16, pp. 329-332, 2017.

[87] N. Mishra, D. K. Choudhary, R. Chowdhury, K. Kumari, and R. K. Chaudhary, "An Investigation on Compact Ultra-Thin Triple Band Polarization Independent Metamaterial Absorber for Microwave Frequency Applications", *IEEE Access*, Vol. 5, pp. 4370–4376, 2017.

[88] H. E. Su, J. L. Li, and L. Xia, "A Novel Temperature Controlled Broadband Metamaterial Absorber for THz Applications", *IEEE Access*, Vol. 7, pp. 161255–161263, 2019.

[89] S. K. Ghosh, S. Das, and S. Bhattacharyya, "A Graphene Based Broadband Metasurface Absorber in the Terahertz Region", *2019 URSI Asia-Pacific Radio Science Conference (AP-RASC)*, pp. 1-4, 2019.

[90] T. Cao, C. W. Wei, R. E. Simpson, L. Zhang, and M. J. Cryan, "Broadband polarization-independent perfect absorber using a phase-change metamaterial at visible frequencies", *Scientific Reports*, Vol. 4, no. 3955, pp. 1–8, 2014.

[91] S. Cao et al., "Two-dimensional subwavelength meta-nanopillar array for efficient visible light absorption", *Applied Physics Letters*, Vol. 102, no. 16, pp. 161109, 2013.

[92] Z. Liu et al., "Automatically acquired broadband plasmonic metamaterial black absorber during the metallic film-formation", *ACS Applied Materials & Interfaces*, Vol. 7, no. 8, pp. 4962–4968, 2015.

[93] M. Luo, S. Shen, L. Zhou, S. Wu, Y. Zhou, and L. Chen, "Broadband, wide-angle, and polarization-independent metamaterial absorber for the visible regime", *Optics Express*, Vol. 25, no. 14, pp. 16715–16724, 2017.

[94] W. Zhu et al., "Wideband visible-light absorption in an ultrathin silicon nanostructure", *Optics Express*, Vol. 25, no. 5, pp. 5781, 2017.

[95] M. H. Heidari and S. H. Sedighy, "Broadband wide-angle polarization-insensitive metasurface solar absorber", *Journal of the Optical Society of America A*, Vol. 35, no 4, pp. 522-525, 2018.

[96] S. K. Ghosh, V. S. Yadav, S. Das, and S. Bhattacharyya, "Tunable Graphene-Based Metasurface for Polarization Independent Broadband Absorption in Lower Mid-Infrared (MIR) Range", *IEEE Transactions on Electromagnetic Compatibility*, Vol. 62, no. 2, pp. 346-354, 2020.

[97] X. Duan, S. Chen, W. Liu, H. Cheng, Z. Li, and J. Tian, "Polarization-insensitive and wide-angle broadband nearly perfect absorber by tunable planar metamaterials in the visible regime", *Journal of Optics (United Kingdom)*, Vol. 16, no. 12, pp. 125107, 2014.

[98] R. Maas, H. Schokker, J. Parsons, and A. Polman, "Experimental Realization of a Coaxial Plasmonic Metamaterial at Visible / UV Frequencies", *Nano Letters*, Vol. 14, no. 11, pp. 7–9, 2013.

[99] M. Desouky, A. M. Mahmoud, and M. A. Swillam, "Silicon based mid-IR super absorber using hyperbolic metamaterial", *Scientific Reports*, Vol. 8, no. 2036, pp. 8–15, 2018.

[100] P. Wu, C. Zhang, Y. Tang, B. Liu, and L. Lv, "A perfect absorber based on similar fabry-perot four-band in the visible range", *Nanomaterials*, Vol. 10, no. 3, pp. 488, 2020.

[101] P. Moitra et al., "Large-Scale All-Dielectric Metamaterial Perfect Reflectors", *ACS Photonics*, Vol. 2, no. 6, pp. 692–698, 2015.

[102] H. Ma, K. Song, L. Zhou, and X. Zhao, "A naked eye refractive index sensor with a visible multiple peak metamaterial absorber", *Sensors*, vol. 15, no. 4, pp. 7454–7461, 2015.

[103] K. Du, Q. Li, W. Zhang, Y. Yang, and M. Qiu, "Wavelength and thermal distribution selectable microbolometers based on metamaterial absorbers", *IEEE Photonics Journal*, Vol. 7, no. 3, 2015.

[104] T. Alam, M. R. I. Faruque, and M. T. Islam, "A double-negative metamaterial-inspired mobile wireless antenna for electromagnetic absorption reduction", *Materials*, Vol. 8, no. 8, pp. 4817–4828, 2015.

[105] M. Bağmancı, M. Karaaslan, E. Ünal, O. Akgol, and C. Sabah, "Extremely-broad band metamaterial absorber for solar energy harvesting based on star shaped resonator", *Optical and Quantum Electronics*, Vol. 49, no. 257, 2017.

[106] B. Mulla and C. Sabah, "Multiband Metamaterial Absorber Design Based on Plasmonic Resonances for Solar Energy Harvesting", *Plasmonics*, Vol. 11, no. 5, pp. 1313–1321, 2016.

[107] H. Lin et al., "Plasmonic absorption enhancement in graphene circular and elliptical disk arrays," *Materials Research Express*, Vol. 6, no. 4, pp. 045807, 2019.

[108] W. Li and J. Valentine, "Metamaterial perfect absorber based hot electron photodetection", *Nano Letters*, Vol. 14, no. 6, pp. 3510–3514, 2014.

[109] R. Schmidt and A. Webb, "Metamaterial Combining Electric- and Magnetic-Dipole-Based Configurations for Unique Dual-Band Signal Enhancement in Ultrahigh-Field Magnetic Resonance Imaging", *ACS Applied Materials & Interfaces*, Vol. 9, no. 40, pp. 34618–34624, 2017.

[110] J. Grant, M. Kenney, Y. D. Shah, I. Escorcia-Carranza, and D. R. S. Cumming, "CMOS compatible metamaterial absorbers for hyperspectral medium wave infrared imaging and sensing applications", *Optics Express*, Vol. 26, no. 8, pp. 10408, 2018.

[111] M. T. Islam, A. Hoque, A. F. Almutairi, and N. Amin, "Left-handed metamaterial-inspired unit cell for S-Band glucose sensing application," Sensors (Switzerland), Vol. 19, no. 1, pp. 169, 2019.

[112] Z. Yi et al., "Tunable graphene-based plasmonic perfect metamaterial absorber in the THz region", *Micromachines*, Vol. 10, no. 3, pp. 194, 2019.

[113] K. V. Sreekanth et al., “Generalized Brewster Angle Effect in Thin Film Optical Absorbers and Its Application for Graphene Hydrogen Sensing”, *ACS Photonics*, Vol. 6, no. 7, pp. 1610–1617, 2019.

[114] Y. Cheng and F. Chen, “Triple-Band Perfect Light Absorber Based on Hybrid Meta surface for Sensing Application”, *Nanoscale Research Letters*, Vol. 15, no. 103, 2020.

[115] E. Shiles, T. Sasaki, M. Inokuti, and D. Y. Smith, “Self-consistency and sum-rule tests in the Kramers-Kronig analysis of optical data: Applications to aluminum”, *Physical Review B*, Vol. 22, no. 4, pp. 1612-1628, 1980.

[116] Aluminium, mineral raw materials isolated illustration stock photo, iStock by Getty Image, https://www.istockphoto.com/photo/aluminium-mineral-raw-materials-isolated-illustration-gm518501862-90071535, 18/02/2021.

[117] High-resolution STEM-HAADF micrograph of Al atoms viewed along the [001] zone axis, Wikipedia, https://en.wikipedia.org/wiki/Aluminium, 18/02/2021.

[118] Gallium Arsenide single crystal 149.17 grams 99.9999% purity undoped, Smart Elements, https://www.smart-elements.com/shop/gallium-arsenide-single-crystal-149-17-grams-99-999-purity-undoped-new/, 18/02/2021.

[119] Visible spectrum, Wikipedia, https://en.wikipedia.org/wiki/Visible_spectrum, 19/02/2021.

[120] Ismo Lindell, Ari Sihvola, *Boundary Conditions in Electromagnetics*, 1st Edition, Hoboken, New Jersey: John Wiley & Sons, Inc., 2019, pp. 11-17.

[121] Nilotpal, Aman, S. Bhattacharyya, and P. Chakrabarti, “Frequency- and time-domain analyses of multiple reflections and interference phenomena in a metamaterial absorber”, *Journal of the Optical Society of America B*, Vol. 37, no. 3, pp. 586-592, 2020.

[122] E. J. Rothwell, J. L. Frasch, S. M. Ellison, P. Chahal, and R. O. Ouedraogo, “Analysis of the Nicolson-Ross-Weir method for characterizing the electromagnetic properties of engineered materials”, *Progress in Electromagnetics Research*, Vol. 157, pp. 31–47, 2016.